Metallic Photonic Crystals for Proposed Applications as Thermal Emission Devices

A DISSERTATION
SUBMITTED TO THE FACULTY OF THE GRADUATE SCHOOL
OF THE UNIVERSITY OF MINNESOTA
BY

Nicholas Ryan Denny

IN PARTIAL FULFILLMENT OF THE REQUIREMENTS
FOR THE DEGREE OF
DOCTOR OF PHILOSOPHY

Andreas Stein

August 2009

Acknowledgements

I would like to thank the following individuals for their help and support:

Professor Andreas Stein, for without his display of colored materials I would not have chosen to attend the University of Minnesota. His insight, friendship and good nature have given me a wonderful environment to work in and set a standard for me to live by. He also makes a great canoe partner!

Current and former group members of the Stein group for their support and thoughtful discussions: Mr. Carlos Aguirre, Ms. Upsorn Boonyang, Dr. Thuy Chastek, Mr. Matthew Dubay, Dr. Nicholas Ergang, Ms. Melissa Fierke, Dr. Sangjin Han, Mr. Phil Jarzombeck, Dr. Kyu Tae Lee, Mr. Fan Li, Mr. David Josephson, Dr. Justin Lytle, Mr. Nicholas Petrovitch, Mr. Yuqiang Qian, Ms. Katie Scholz, Dr. Jung Ho Son, Mr. Ryan Turgeon, Mr. Anh Vu, Dr. Zhiyong Wang, Dr. Hongwei Yan, Mr. Danhui Ye, Mr. Won Cheol Yoo and Mr. Dan Yu. I would like to especially thank Dr. Justin Lytle and Dr. Nicholas Ergang for all their input and being wonderful mentors and friends throughout the years.

Professor David J. Norris, Dr. Sang Eon Han and Mr. Prashant Nagpal for their numerous insights on my research, invaluable help and access to their laboratory.

Steven and Patricia Denny for being my parents. Without their support and love I would not be where I am today.

Jillian Denny, my wife and confidant. For without her support, care, understanding, patience and love none of this would be possible. Also for her superb cooking. Spectro Electronic Magic!

Dedication

To my wife Jill.

Abstract

Incandescent lighting is highly inefficient. One possible solution is to replace the traditional filament with an ordered photonic crystal filament that will increase the efficiency of the lamp. This work details steps towards the fabrication of such a filament with the fabrication of monolithic three-dimensionally ordered macroporous (3DOM) metallic photonic crystals. The 3DOM metallic materials produced in this work were comprised of W, Mo and alloys of those materials. The 3DOM W materials were produced from the precursors tungsten(VI) chloride, tungsten(V) ethoxide, tungstic acid, peroxotungstic acid, ammonium metatungstate (AMT) and an acetylated peroxotungstic acid (APTA). 3DOM Mo was produced from the precursors ammonium molybdate (AMo) and an acetylated peroxomolybdic acid (APMoA). To fabricate 3DOM W/Mo materials combinations of precursors of AMT and AMo were utilized or a combination of the syntheses APTA and APMoA to create APTA/APMoA was employed. A variety of synthetic conditions were optimized to produce large monolithic pieces of 3DOM W and 3DOM W/Mo with dimensions of up to 1×1×0.3 cm^3. These conditions included varying the solvent mixture, precursor concentrations, reduction conditions and precursor infiltration technique.

The 3DOM metallic monoliths were tested for thermal stability using both joule heating and radiant heating techniques in N_2 atmospheres. Joule heating at 40 W for 15 min destroyed the nanostructure of the material. Radiant heating was employed to study the grain coarsening. At 800 ºC the 3DOM W monolith exhibited grain coarsening and

needle formation caused by H_2O in the system. Needle formation could be eliminated by rigorous evacuation or by the incorporation of Mo as an alloy. 3DOM W/Mo alloys at 95:5 wt% maintained their nanostructure and relative grain size at 800 ºC but were coarsened at 1000 ºC. At both temperatures the material did not produce needles even in the presence of minute amounts of water. The effect of Mo on the nanostructure was studied by in situ TEM heating to 1000 ºC. In 3DOM W/Mo alloys it is postulated that the Mo has a pinning effect on the dislocations in the structure. These methods provide a route towards fabricating 3DOM metallic photonic crystals for thermal emission.

Table of Contents

List of Tables

List of Figures

List of Abbreviations

3DOM	Three-dimensionally ordered macroporous
˚C	Degrees Celsius
α	Alpha
ALD	Atomic layer deposition
AMo	Ammonium molybdate
AMT	Ammonium metatungstate hydrate
APMoA	Acetylated peroxomolybdic acid
APTA	Acetylated peroxotungstic acid
APTA1	Acetylated peroxotungstic acid, Synthesis 1
APTA2	Acetylated peroxotungstic acid, Synthesis 2
APTA/APMoA	Acetylated peroxotungstic acid / acetylated peroxomolybdic acid
Ar	Argon gas
bcc	Body centered cubic
CVD	Chemical vapor deposition
EtOH	Ethanol
EDS	Energy dispersive X-ray spectroscopy
fcc	Face centered cubic
h	Hour
H_2	Hydrogen gas
HCl	Hydrochloric acid
H_2O	Water
H_2O_2	Hydrogen peroxide
λ	Wavelength
L	Liter
M	Molarity
m	Order of Bragg diffraction
min	Minute

mL	Milliliter
mm	millimeter
Mo	Molybdenum
n	Index of refraction
N_2	Nitrogen gas
PDF	Powder diffraction file
PMMA	Poly(methyl methacrylate)
s	Second
SEM	Scanning electron microscopy
TEM	Transmission electron microscopy
θ	Theta
μm	Micrometer
UV–vis	Ultra violet – visible
vol	Volume
ϕ	Volume fraction
W	Tungsten
W_2C	Tungsten carbide
WCl_6	Tungsten(VI) chloride
$W(CO)_6$	Tungsten hexacarbonyl
WO_3	Tungsten(VI) oxide
$W(OEt)_6$	Tungsten(V) ethoxide
wt%	Weight percent
XRD	X-ray diffraction

Chapter 1
Introduction

Outline

1.1. Let there be light and keep the ice caps too!

1.2. Bending light to our will

1.3. 3DOM materials as photonic crystals for thermal emission

1.1. Let there be light and keep the ice caps too!

Global warming, it seems to be about half the news each week. People are looking for ways to "lighten" their carbon footprint on the planet. One of the easiest ways touted today to change your carbon footprint is to merely change your light bulbs from an incandescent bulb to a compact fluorescent lamp (CFL). This is absolutely the easiest change anyone can make, but it does come with a drawback, CFL's contain a small amount of mercury (approximately 4 mg). This mercury content is easily off set by reduced emissions from power plants (the major source of mercury contamination). However, according to a recent study, there is reason to believe that this may not be totally true, especially for areas that do not primarily receive their power from coal-fired power plants.[1] In those areas, broken bulbs could actually lead to an increase in the mercury content in the air. Maybe the answer does not solely lie in CFLs.

Another up and coming technology for the replacement of incandescent lights is based on light emitting diodes (LED). These are the most energy efficient types of lighting commercially available to date. The big draw back with a LED lamp is its price tag. At approximately $60 a bulb, the barrier of initial cost is far too great for the average person to buy one.

This brings us back to the lowly incandescent light bulb. Light bulbs are cheap and do not contain harmful chemicals. The big problem is the 10% efficiency for light output.[2] But what if there was a way to increase that efficiency?

1.2. Bending light to our will

A little over 20 years ago, Yablonovitch and John independently postulated that a periodic material comprised of high and low refractive indexes could modify its spontaneous emission based on its periodic structure.[3,4] Periodic materials of differing refractive indexes are called photonic crystals. Photonic crystals exhibit a property called a photonic bandgap. A photonic bandgap is analogous to a bandgap in a semiconductor. In a photonic crystal, photons instead of electrons are forbidden to propagate through a material at specific wavelengths based on the band structure.[3,4] This effect can be described by a combination of Bragg's Law and Snell's Law.[5,6] If the photonic and electronic bandgaps overlap in energy for a photonic crystal, this can increase the wanted emission while decreasing unwanted emissions thus changing the performance of lasers, thermophotovoltaic cells or even blackbody emitters (light bulbs) for example.[5] For materials with a face-centered-cubic (fcc) lattice a refractive index contrast of 2.8 times needs to be observed to produce a full photonic bandgap.[7] If the refractive index contrast is lower than 2.8 times or the structure is not perfectly formed, a stop band is produced. Stop bands are incomplete photonic bandgaps where the band structure does not exhibit a bandgap across all reciprocal space.[5,6]

For a light bulb then it might be possible to fabricate a filament which incorporates a photonic crystal that would forbid the emission of the unwanted infrared (heat) emission and thus make the light bulb more efficient. Recently Lin et al. fabricated a woodpile

photonic crystal comprised of tungsten to achieve that goal.[8-14] The woodpile consists of a series of logs spaced approximately one thickness apart with each subsequent layer perpendicular and every other layer offset so that the logs are over the spaces of the previous layer of the same direction. The tungsten photonic crystal produced by Lin et al. was able to achieve a complete bandgap beginning at 2 μm and down in energy. The tungsten photonic crystal fabricated by Lin et al. also produced an emission spectrum with a decreased intensity in the infrared.

Also recently von Freymann et al. were able to produce a tungsten photonic crystal with an inverse opal morphology.[15] These materials were produced by a self assembly technique of silica spheres which formed a face-centered-cubic array. The material was then infiltrated with tungsten by chemical vapor deposition (CVD). These materials exhibited stop bands which are incomplete bandgaps. One property of CVD is that it fully coats the template material. Normally this is a very sought after result but for photonic crystals a more open structure is desired than that produced by CVD.[16] Here the tungsten inverse opal stop bands diminished as the tungsten coating became thicker and prevented light from penetrating into the structure.

1.3. 3DOM materials as photonic crystals for thermal emission

The focus of this thesis will be to create a photonic crystal for use as a thermal emission device. To produce photonic crystals, three-dimensionally ordered macroporous (3DOM) materials will be employed. 3DOM materials are formed from colloidal crystals, and in

this work the colloidal crystals were comprised of poly(methyl methacrylate) (PMMA) spheres (Figure 1.1 A). The PMMA spheres sediment into a fcc array, i.e., an ordered periodic structure.[17] The 3DOM materials produced from the colloidal crystal have a bicontinuous network of walls and macropores (voids), and the macropores are connected by windows where the spheres once touched (Figure 1.1 B). When referring to dimensions of walls in this work, it will be referring to the dimensions of the thin struts as seen in the 3DOM W sample in Figure 1.1 B that connect the previous octahedral and tetrahedral void spaces from the fcc array.

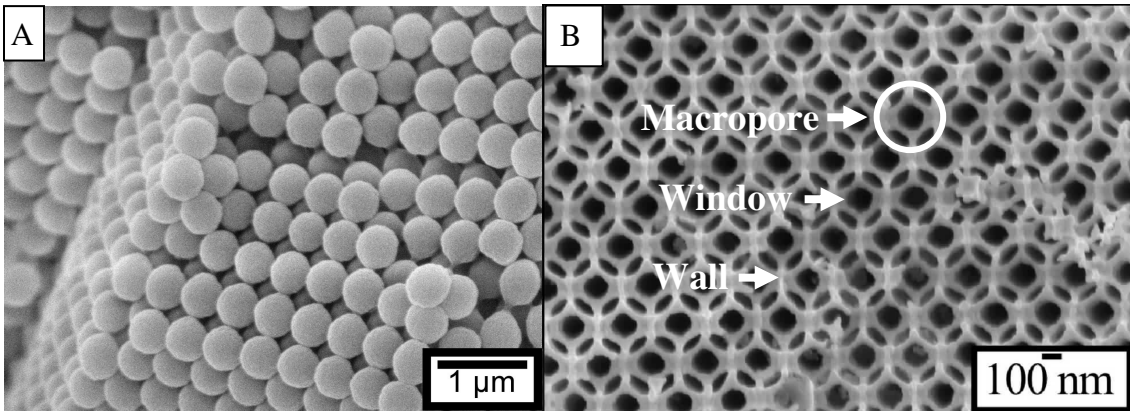

Figure 1.1. (A) SEM image of a colloidal crystal comprised of a fcc array of poly(methyl methacrylate spheres). (b) SEM image of 3DOM W depicting the macropore, window and wall structural features.

In this work a suitable precursor material will need to be selected to produce a highly open 3DOM structure. Tungsten and molybdenum precursors will be investigated. The corresponding metallic phases produced after reduction exhibit high melting temperatures, making them ideal materials for thermal emission over a broad range of

temperatures.[18] As well, synthetic conditions will need to be optimized so that monolithic samples are produced over granules as the samples will need to be resistively heated. Granules are the most common morphology of 3DOM materials that consist of a powder or sand like consistency and range in size from 10s to 100s of μm.[19,20] Here monoliths will need to be fabricated with at least one dimension around 1 cm to be used as a filament and the rest of the material being large and robust enough to be placed in the thermal emission device without structural failure. Monoliths have dimensions around 2 to 10 mm in dimension for height, width and length. Only two other 3DOM materials have been produced in monolithic form, silica[21] and carbon[22]. Free standing thin films only 10s of μm thick are not considered monoliths for this work. Partial monoliths are sometimes produced when, as a result of deficiencies in infiltration, the monoliths are not fully formed in the top or middle portions and form a bowl with side walls a few mm in thickness. Partial monoliths easily fracture and are not suited for use as a filament. Each monolith and granule is comprised of ordered domains which are areas of continuous order inherited from the template material usually 1 to 10s of μm in size. Grains refer to the crystalline materials and are usually on the order of 10s of nm. Furthermore the structures produced will have to be sufficiently open to exhibit photonic stop band effects.[16]

In this work the optimization of the fabrication of 3DOM W and 3DOM W/Mo photonic crystals will be discussed in chapter 3. The initial testing of 3DOM W and 3DOM W/Mo as filaments is outlined in chapter 4. As well, the results of radiative heating and the

fabrication of a W/Mo alloy are discussed in chapter 4. In chapter 5, a study of the grain coarsening by TEM and in situ heating of 3DOM W and 3DOM W/Mo will be discussed. The next chapter will consist of a short review on lighting, photonic crystals and 3DOM materials.

Chapter 2

A Look Back

Outline

2.1. Bright ideas

- 2.1.1. Incandescent lighting in a flash
- 2.1.2. Light from the other side

2.2. Photonic crystals

- 2.2.1. Building up and down photonic crystals
- 2.2.2. 1D photonic crystals
- 2.2.3. 2D photonic crystals
- 2.2.4. 3D photonic crystals

2.3. Colloidal crystals and 3DOM materials

- 2.3.1. Colloidal crystals
- 2.3.2. 3DOM materials
  - 2.3.2.1. 3DOM metallic materials
  - 2.3.2.2. 3DOM photonic properties

2.4. Tungsten photonic crystals

2.1. Bright ideas

2.1.1. Incandescent lighting in a flash[23-25]

The creation of the electric light bulb began in 1809 when Joseph Wilson Swan produced the first arc lamp using two carbon filaments. In 1820, Warren De la Rue, using a Pt wire, produced an incadenscent lamp but this lamp proved to be “slightly” cost ineffective, similar to the LED today.

Innovations continued until 1879 when Thomas A. Edison and Joseph Wilson Swan independently invented the evacuated carbon filament light bulb and then joined together to bring that invention to the world. The carbon filament had a few upgrades including the use of bamboo as the filament materials. However the voltage was low and the light produced was not very bright.

A number of other materials were used as filaments before tungsten, including osmium and tantalum which both produced an increase in the amount of light produced. The first tungsten filament was produced in Hungary by A. Just and F. Hanaman from the starting materials of tungsten powder, sugar and gum in 1903. From 1903 to 1909 William D. Coolidge and the General Electric Company perfected the synthesis of ductile tungsten for use as a filament as it is known today. However the incandescent bulb was still evacuated and only produced light at lower power. At higher power and temperature, the filament continued to evaporate and coat the glass enclosure.

Using ductile tungsten, another researcher at the General Electric Company by the name of Irving Langmuir was able to produce the light bulb as we know it today in 1916. He combined the use of argon as an inert fill gas and a coiled filament to optimize the system for long life and high intensity output.

Since the optimization of the system in 1916 by Langmuir, there have been no appreciable changes in the incandescent tungsten filament. The fill gas can be changed to krypton to lengthen the life of the bulb. Halogen gases are also used to produce a higher light output by allowing the filament to be heated to a higher temperature. A halogen bulb can be operated at higher temperatures because the increased amount of evaporated tungsten is complexed with the halogen gas before it can deposit on the glass bulb to form a tungsten-halogen compound. When the tungsten-halogen compound is near the filament again, the heat dissociates the compound and the tungsten is returned to the filament.

Other improvements are now primarily done to the glass enclosure. A fine silica powder can be sprayed on the inside of the glass to soften the light.[2] In the Reveal™ bulb from GE, niobium is incorporated in the glass to filter out the yellow tinge of the incandescent filament. Efforts aimed at increasing the efficiency of incandescent lights have involved the application of an infrared coating on the bulbs.[26,27]

The next big step for incandescent light bulbs, not associated with photonic crystals and the work in the following chapters, could be one of two things. 1) A throw back to the use

of carbon as the filament where carbon nanotubes are being used to produce incandescent lighting with a higher efficency.[28] 2) A total ban of incandescent light bulbs with the goal of reducing green house gas emissions.[29] Australia has a ban on selling incandescent bulbs that goes into effect in 2010.

2.1.2. Light from the other side[23]

Besides incandescent lamps, a large variety of other types of lighting devices are commercially available. Most notable are the fluorescent lamps which are the standard at most commercial sites because of their lower energy consumption. The compact fluorescent lamp or CFL is probably the most widely known type of fluorescent lamp due to its media exposure over the last few years and is primarily used in residences. Other lamps commonly seen are at stadiums and street lights which can be high-pressure mercury lamps, metal-halide lamps and high- and low-pressure sodium lamps. The last major form of lighting devices is light emitting diodes (LED). These are fast becoming the new standard for almost every application but homes as the total cost of use becomes competitive with the more traditional lighting sources. One of the more visible uses is in stop lights.

2.2. Photonic crystals

It is always interesting how the scientific community mimics nature. Research in photonic crystals is no different. Long before Yablonovitch and John proposed that photonic crystals could be formed from a periodic array of materials[3,4], nature had

already perfected the art. In butterfly wings, some of the color is produced by periodic arrays of holes in the scales that form a diffraction grating which reflects selected wavelengths of light.[30,31] In opals, the light flashes off the ordered arrays of silica spheres that constitute the nanostructure of the opal.[32,33]

2.2.1. Building up and down photonic crystals

There are three basic ordered structures of photonic crystals; 1D, 2D and 3D. Each ordered structure type has a basic building block. A 1D photonic crystal can be thought of as infinite planes of alternating materials stacked on top of each other, similar to a very large stack of 2 kinds of pancakes. 2D photonic crystals are usually arrays of structures like rods where the height is approximated to be infinite, similar to a symmetrical tree farm. 3D photonic crystals can be visualized as stacks of arrays, similar to ping pong balls tightly packed into a box. The methods for producing photonic crystals fall into one of two methods, top down or bottom up fabrication.

Both 1D and 2D photonic crystals primarily use top down methods for fabrication. Top down techniques usually deposit a layer of material on a substrate and then, employing various techniques, selectively remove portions of the material. Most notably these techniques include lithography, focused ion beams (FIB) and etching. For 1D photonic crystals the techniques are primarily deposition of materials in a layer by layer synthesis or multiple layers of polymer films. 2D photonic crystals employ many techniques to achieve the array patterns needed to produce the photonic effects. These include

lithography, FIB, etching and films comprised of a monolayer of colloidal crystals. For 3D photonic crystals, these techniques are possible but can be time consuming and/or expensive to complete. Many of the 2D and 3D materials produced are then used as templates and infiltrated with the photonic crystal material of choice.

On the flip side, bottom up fabrication techniques are primarily employed to fabricate 3D photonic crystals. Here instead of taking a bulk material and carving away the unwanted material, building blocks are assembled to produce the photonic crystals or templates. The most notable technique is colloidal crystal self assembly. 2D photonic crystals can be formed using colloidal crystals if a monolayer of material is deposited. For 3D photonic crystals a variety of methods are available to produce the colloidal crystals which include sedimentation, convective self assembly, vertical deposition, confinement and spin coating.

2.2.2. 1D photonic crystals

1D photonic crystals can be comprised of both sheets of materials or a single array of features (i.e. a series of holes in a line). Recently it was proposed that an array of 1D photonic crystals could achieve greater selectivity in biomolecular detection.[34] By using an array of 1D photonic crystal with varying lattice constants a sensor with a higher selectivity was produced.

By tapering down the spacing of the edges of Bragg mirrors (vertical slits in a material), an increased transmission and flatter passbands was observed.[35] This allowed for a narrower emission which is optimal for applications for information transmission.

2.2.3. 2D photonic crystals

2D photonic crystals comprised of a many different of materials are produced by a variety of methods. Some notable methods are lithography, FIB, etching and films comprised of a monolayer of colloidal crystals. Some of the first techniques used to produce 2D photonic crystals involved lithographic techniques to apply masks and then etching to remove sections of the underlying material. To produce a GaAs 2D photonic crystal with a hexagonal array of air holes, a nickel mask containing holes was patterned on the surface of a GaAs film 600 nm thick, and then reactive ion etching with $SnCl_4$ was performed to remove GaAs to create the array of air holes.[36]

2D photonic crystals are also studied in the lighting field. Photonic crystals on the surface of organic light emitting diodes (OLED) can help to boost the efficiency.[37] An array of SiO_2 rods was fabricated on the surface of an OLED by using a photo resist mask and etching the SiO_2 away. Comparison of the output efficiency of the OLED, with and without the 2D photonic crystal, revealed a 50% increase in efficiency.

Colloidal crystals can be used as a template for the formation of 2D photonic crystals when a monolayer of colloidal particles is assembled on a substrate. Recently a ZnO

photonic crystal was formed using a colloidal crystal template.[38] An array of polystyrene (PS) spheres (488 nm) was assembled, and nanorods of ZnO were formed from aqueous methods after the addition of a seed layer. The photonic crystal exhibited a photonic band gap at 437 nm.

Molding can also be an effective method to produce photonic crystals. Nanoimprinting of PMMA was achieved by using a SiO_2 mold.[39] To produce the mold a monolayer of PS spheres was deposited onto a SiO_2 film. The spheres were then etched to reduce the diameter of the spheres and produce a mask for the SiO_2. After etching and removal of the spheres an array of SiO_2 pillars was achieved. This array could then act as a mold and be infiltrated with PMMA and then striped off to produce a 2D PMMA photonic crystal.

Another way to produce a mold is to employ FIB. In a recent study, FIB was used to create a bull's eye pattern on a Si substrate.[40] Here FIB was able to create an ultra smooth mold where metals were evaporated onto the surface to form a thin film. Continued deposition of metals or an epoxy film was applied to the thin film to facilitate the removal of the sample from the mold. This technique was also translated to other structures such as pyramids and ridges.

An interesting property of 2D photonic crystals is also is ability to function as a wave guide. If a photonic crystal has a defect through its structure, the photons can be forced to propagate along that defect similar to a fiber optic cable.[5] It was reported that such a

waveguide can even bend light at 90º angles.[41] To achieve this, an array of GaAs rods was fabricated with a channel containing a 90º bend. When the correct frequency of radiation was applied to the structure a transmittance of >95% was seen through the bend. More recently it was determined that by increasing the refractive index contrast ratio to 7.6, a waveguide with two 60º bends can achieve a >90% transmission of the incident radiation.[42]

2.2.4. 3D photonic crystals

3D photonic crystals are often produced by first forming a sacrificial template material. The template material can be prepared through a variety of methods but it can be simplified to lithographic and colloidal crystal techniques. It should be noted that there are materials where the template material has a higher refractive index due to material doped or incorporated into the template structure so that the template then acts as the photonic crystal.[43] Another method to create 3D photonic crystals is to "drill" out a block of material by reactive ion etching.[44]

To create 3D photonic crystals through lithography a photoresist is usually employed.[45] A photoresist is a polymer that undergoes an irreversible chemical reaction when exposed to light.[5] Exposure to light either renders the polymer soluble (positive photoresist) or insoluble (negative photoresist) and creates a pattern by using a mask. The 3D structure of the photoresist can also provide a good support for materials to be templated on to the support. Recently it was reported that TiO_2 can be electrodeposited onto a photoresist of

SU–8 on an ITO–coated substrate.[46] The SU–8 in this structure was fully filled and then the template was removed to achieve an inverse structure comprised entirely of TiO_2.

Different surface orientations can also be achieved by manipulating the light that interacts with the photoresist.[47,48] Face-centered-cubic (fcc) structures with both $\bar{a}\bar{a}$(111) and (811) orientation were produced by altering the light with a prism. Other changes to 3D photonic crystals occur in the form of induced defects to increase the functionality of the materials.[49]

As the use of colloidal crystals is an important subject of this thesis it will be covered in its own section.

2.3. Colloidal crystals and 3DOM materials

2.3.1. Colloidal crystals

Colloidal crystals are materials comprised of any orderly packed material of nearly identical particles with colloidal dimensions (nanometers to micrometers). Almost all colloidal crystals are comprised of spherical particles due to the ease of synthesis and uniformity. The most common colloidal crystal known is the opal, it is comprised of a fcc array of silica spheres that exhibit photonic crystal properties.[32,33] As opals are comprised of colloidal crystals it is common to call a colloidal crystal of spheres an opal and structures formed using it as a template, inverse opals. In this work we will refer to inverse opals as three-dimensionally ordered macroporous (3DOM) materials. In the

laboratory there are three common compositions of colloidal crystals; polystyrene[50], silica[51] and poly(methyl methacrylate)[52]. The three types can be lumped into two kinds, latex and silica spheres. There are pros and cons to both systems. When using silica spheres the template can withstand higher infiltration temperatures for techniques like chemical vapor deposition (CVD) or if a precursor needs to be sintered before forming a permanent structure. However, the only removal method of silica spheres is through etching the spheres away. Latex spheres can be synthesized in large batches and can result in colloidal crystals in a one step process. If the 3DOM material needs to be heated to form its intended phase, the template can be removed during this step as well. However the low glass transition temperature of these materials (105 ºC) makes them ill suited for higher temperature synthesizes.

The fabrication of a colloidal crystal from either latex spheres or silica spheres can be obtained through similar methods. These methods include sedimentation, convective self assembly, vertical deposition, confinement and spin coating.[53] Sedimentation can be achieved through gravity or centrifugation methods which form very similar materials.[52] The big difference between gravity and centrifugation techniques is the time required to form the colloidal crystal. For sedimentation techniques the time can be up to a few months whereas centrifugation sediments samples in the span of a few hours. However there is evidence that the order of the colloidal crystals produced by gravity sedimented products is greater, meaning that there are fewer defects in the colloidal crystal structure.[54]

Convective self assembly involves a substrate placed in a colloidal crystal suspension with a temperature gradient present in the suspension.[55,56] As the solution evaporates, a colloidal crystal forms at the interface of the solvent and the substrate surface through capillary forces. The thickness of the colloidal crystal film created can be controlled by the concentration of spheres in suspension and by the evaporation time which is both solvent and temperature dependent.

Vertical deposition is similar to convective self assembly, but in vertical deposition the substrate is drawn out of the colloidal suspension.[57] The thickness of the colloidal crystal here can be tuned with the draw rate. Monolayers to thicker films, with a set number of layers, can be achieved by drawing the substrate multiple times from the colloidal suspension.

Confinement methods are an interesting development where the colloidal crystal is formed inside of a mold.[58] The mold is usually a micro-capillary plane where two glass slides are close together and solvent can evaporate around the edges. This produces colloidal crystals with a predetermined thickness.

Another technique to produce colloidal crystals quickly is spin coating.[59] Here a substrate is spun at high a rate and a drop of colloidal suspension is placed in the center. The droplet quickly spreads out and dries forming a thin film colloidal crystal on the surface

of the substrate. This is a quick and easy method for producing monolayers to thin films of colloidal crystals but the overall order of the system is not always optimal.

2.3.2. 3DOM materials

Using a colloidal crystal as a template material, 3DOM materials can be realized. The methods for producing the 3DOM materials is almost limitless. These methods include the use sol-gels[60-62], CVD[15,63,64], atomic layer deposition (ALD)[65], electrodeposition[66,67] and core shell[68,69]. Each technique has its limitations. Sol-gels primarily produce granular samples with only a few materials forming highly extended monolithic structures.[21,22] CVD and ALD are similarly limited in the infiltration depth and typically only thin film structures are formed. Electrodeposition has a unique problem where the deposition becomes preferential in a particular region and then the filling of the opal structure ends in all other regions. Core shell structures are only limited by the fabrication of the core shell material itself. The surface coating needs to be uniform throughout to facilitate proper packing of the materials.

Mesoporous features can also be incorporated into the wall structure of the 3DOM SiO_2 for example.[61] The type of secondary template used and its interactions with the colloidal crystal can also change the alignment of the mesopores from perpendicular to parallel to the sphere surface.

2.3.2.1. 3DOM metallic materials

The focus of this work is to produce metallic 3DOM materials from W and Mo. Other metallic materials have also been produced. Sb 3DOM metallic materials were produced that exhibited full photonic bad gaps and both the metallicity gap and the optical gap.[70] As well, metal containing salt solutions can be precipitated to create 3DOM Ni, Co, Fe and a NiCo alloy after reduction.[71]

A number of groups have worked on fabricating gold into a matrix by gold-silica[72] core-shell materials and then co-sedimenting the core-shell materials to produce 3DOM materials. The 3DOM Au core-shell structures then exhibit stop bands that cannot only be shifted by changing the pore size but by also changing the core-shell thicknesses. Another method to obtain a similar result is to infiltrate a silica colloidal crystal with gold nanoparticles and then fill in the interstitial area with a polymer matrix.[73] After template removal, similar photonic effects can be seen as in the previous sample. Similarly, 3DOM Au structures were produced by the co-deposition of gold nanoparticles and the colloidal template.[74] The ordered structure of the metallic photonic crystal resulted in an enhanced SERS signal.

A great variety of metallic 3DOM materials can also be produced by electrochemical methods. These include Au[75,76], Ni[77], Ag,[78] Cu and Pt.[79] Using electrodeposition to produce these materials is a delicate operation where the experiments are usually pulsed so that the metal ions in solution can diffuse into the interstitial areas for continued

deposition. If this is not done, the deposition can easily build up in one region so that the colloidal crystal is not fully infiltrated. Also the surface termination can be varied, which can then affect the plasmon modes.[76] 3DOM metallic materials can also be achieved by electroless deposition to produce 3DOM Ni, Cu, Ag, Au and Pt.[80]

Also interesting are metallic opals produced by first creating a silica inverse opal from PS and then electroplating gold into the void space to form an opal.[81] Gold opals have also been fabricated using 3DOM Ni materials.[82] Sphere arrays have also been produced by creating 3DOM C and adding metals via molten methods to get structures comprised of Pb, Bi, Sb and Te.[82]

2.3.2.2. 3DOM photonic properties

The photonic properties of 3DOM materials are based on Bragg diffraction (Equiation 2.1).[6] Just as in a crystalline lattice, a lattice with periodic features and dimensions on the same order of magnitude as the wavelength of visible light or infrared radiation will constructively reflect radiation, forbidding it to propagate through the structure and will form bandgaps or stop bands.[5] To better define the interactions, Snell's law (Equation 2.2) is also incorporated into Bragg's Law to account for the change in indexes of refraction (Equation 2.3).[83,84] Here m is the order of Bragg diffraction, λ is the wavelength at the stop band minimum, n is the refractive index and θ is the angle of incidence from normal. Here, n_{avg} can be expanded into two parts, the wall and voids where ϕ is the volume fraction of the walls (Equation 2.4).

$$m\lambda = 2d \sin^2 \theta \qquad \text{Equation 2.1}$$

$$n_1 \sin\theta_1 = n \ \sin\theta_2 \qquad \text{Equation 2.2}$$

$$\lambda = \frac{2d}{m}\sqrt{n_{avg}{}^2 - \sin^2\theta} \qquad \text{Equation 2.3}$$

$$n_{avg} = \phi n_{walls} + (1-\phi) n_{voids} \qquad \text{Equation 2.4}$$

In addition, dynamic diffraction theory can be incorporated into the equation to account for scattering. However for this purpose the above Equation 2.4 gives a close enough approximation for the stopbands. It can now be seen that by changing the template size of the material (which effects *d*) that the λ of the stop band can be shifted. This is how the 3DOM metallic materials can be tuned to the infrared from the more common visible spectrum.[6] The λ can also be affected by changing the refractive index of the walls or voids but in this study that is not very variable due to the temperature requirements.

Metallic photonic crystals also exhibit a metallicity gap.[85] This occurs when the wavelength of radiation is much longer than the periodicity of the metallic material. In these cases the plasma frequency of the material determines the optical properties, which means that any frequency below the plasma frequency will have no absorption. Or stated

another way, no photon states below the plasma frequency exist creating a metallicity gap. If the bandgap is tailored to overlap with the metallicity gap a much larger photonic band gap can be observed for a metallic material.

2.4. Tungsten photonic crystals

The first major advance in tungsten photonic crystals came in 2002 with the tungsten woodpile structure produced by CVD.[8] This structure exhibits a full photonic bandgap starting at 5 μm and up in wavelength. Lin et al. have continued to advance this structure through out the past few years and have been able to expand the photonic bandgap down to 1.5 μm.[12] As well, they have reported that the emission from this material has a reduced infrared signal and narrow band emission.[9,10,12] The reduced emission can also be achieved by 2D W photonic crystals.[86] Wan et al. determined that a 2D photonic crystal can exhibit a more efficient emission but a more selective range of suppression requires a thicker 3D photonic crystal.[87]

Von Freymann et al. reported an inverse opal (fcc) W photonic crystal.[15] The materials made in this study exhibited a less intense photonic stop band as the wall thickness of the structure was increased.

However, theoretical studies have predicted that photonic effects can be achieved with a fcc array of voids if the structure is sufficiently open.[16,88] Moreover, the photonic

properties are affected by slight defects in the structure of the system that diminish those properties.

Chen et al. recently reported a 3DOM W material produced from WO_3.[89] The 3DOM W produced exhibited reduced photonic effects due to very rough pore walls and closed windows, which is in agreement with previous work[6,15,16].

Recently, Walsh et al. expanded on the W woodpile structure by coating the structure with Ir by ALD.[14] This allowed the band edge to be shifted from 1.6 μm to 0.9 μm by coating the W structure with 40 nm of Ir.

Over the past few years, tungsten photonic crystals have been theorized to work well as thermophotovoltaic devices.[90,91] Nagpal et al. have shown that their tungsten woodpile structures will produce a narrow band emission that can have a 30% increase in the efficiency of the solar cell. [91]

Chapter 3

Fabrication of 3DOM Metallic Photonic Crystals.

Outline

3.1. Introduction

Metallic photonic crystals used for enhanced thermal emission devices need to be robust enough to withstand the demands that are exerted on them. One property of these materials to take into consideration was the melting temperature of the emitter. As the initial scope of their project was to create a more efficient light bulb, materials that could survive 2500+ ºC were chosen. Both tungsten and molybdenum were good candidates for this application as the melting points are 3422 ºC and 2623 ºC respectively.[18] Theoretical calculations on three-dimensionally ordered macroporous (3DOM) structures comprised of tungsten and molybdenum state that this periodic structure is suitable for modifying the thermal emission.[16] Other structures comprised of tungsten have been produced including the woodpile structure that exhibits a large photonic bandgap.[12] These materials, however, require more expensive equipment and complex techniques for production including lithographic techniques, etching and CVD. The techniques employed in this study are less complex and can be performed on the bench top. Furthermore, the poly(methyl methacrylate) (PMMA) template was produced by self assembly, thus cutting down on the initial cost of the project. Inverse opals comprised of tungsten have also been produced using silica spheres and CVD infiltration.[15] The tungsten inverse opal exhibited stop bands but with thicker walls the stop bands diminished in intensity. The loss of photonic properties was a direct result of the smaller

window sizes between adjacent macropores produced by the CVD method, but if the window size could be increased, the photonic properties would not be diminished.[16] In this chapter a method for producing 3DOM tungsten with large window sizes to retain photonic properties will be discussed. The fabrication of 3DOM molybdenum will also be detailed below.

3.2. Experimental

3.2.1. Materials

The following chemicals were used as–received: molybdenum powder (99.9+%, 1–2 μm), tungsten powder (monocrystalline, 99.9+%, 0.6–1 μm) and tungsten(VI) chloride (99.9+%) from Aldrich Chemical Company; tungsten(V) ethoxide (95%) from Gelest; methanol (99.9%) from Fisher Scientific; ammonium metatungstate hydrate (AMT) (≥99.0% as WO_3) from Fluka; tungstic acid from J.T. Baker; ammonium molybdate tetrahydrate, concentrated hydrochloric acid (37.3%), glacial acetic acid (99.9%) and hydrogen peroxide (30%) from Mallinckrodt Chemicals; forming gas 10%:90% H_2:N_2 from Oxygen Service Supply; ethanol (200 proof, anhydrous) from Pharmco-AAPER and Commercial Alcohols; H_2 (industrial) from the University of Minnesota, U–Stores. Millipore water with a resistivity 18.2 MΩ–cm was used. N_2 was obtained from the University of Minnesota house system.

3.2.2. Preparation of tungsten precursors

3.2.2.1. Tungsten(VI) chloride (WCl_6)

In a N_2 atmosphere, 3.96 g of WCl_6 was dissolved in a mixture of 15.42 g methanol and 0.82 g concentrated HCl to produce a yellow solution which was then used for infiltration into the colloidal crystal template. Exposure to O_2 should be minimized to avoid oxidation to WO_3 at this stage.

3.2.2.2. Acetylated peroxotungstic acid (APTA)

3.2.2.2.1. Synthesis 1 (APTA1)

The APTA synthesis was adapted from Sharma, et al.[94] In a three–necked 100 mL round bottom flask, 5 mL of 30 wt% H_2O_2 was cooled to 0 ºC with stirring. The reaction vessel was purged with N_2 for a period of 15 min. Subsequently, 0.94 g of tungsten powder was added in small aliquots over a period of 10 min, maintaining the pyrophoric metal powder in an inert atmosphere during this time. Caution: cooling was important at this stage, because the reaction of tungsten and H_2O_2 was exothermic and would occur too rapidly at room temperature. When all tungsten had been added, the ice bath was allowed to warm up to room temperature. The tungsten remained unreacted until the temperature reached approximately 10 ºC. After the tungsten had fully reacted, the resulting peroxotungstic acid solution was clear and colorless or tinted slightly yellow (if the acetylating step is skipped peroxotungstic acid can be obtained). To improve the solubility of peroxotungstic acid in polar solvents like methanol, 5 mL of glacial acetic acid was added to acetylate the peroxotungstic acid. The solution was then heated to 55

ºC for a period of 3–6 h with a condenser attached. Solvent was removed by heating at 60 ºC and a white powder was recovered. The powder was dissolved in methanol or a H_2O:methanol mixture (4:1 vol:vol). The resulting solution was then filtered to remove any solid contaminants such as tungsten oxides, using a Whatman 0.2 μm syringe filter. The filtered solution was used as a precursor solution. The FT–IR spectrum of the APTA product was consistent with the published spectrum.[94]

3.2.2.2.2. Synthesis 2 (APTA2)

The second APTA synthesis was adapted from Cronin, et al.[95] In a 250 mL round bottom flask, 60 mL of 30 wt% H_2O_2 were combined with 60 mL of glacial acetic acid and cooled to 0 ºC with stirring. Tungsten powder (5 g) was added to the cooled solution in small aliquots over a period of 10 minutes. Caution: cooling was important at this stage, because the reaction of tungsten and H_2O_2 was exothermic and would occur too rapidly at room temperature. When all tungsten had been added, the ice bath was allowed to warm up to room temperature. The tungsten remained unreacted until the temperature reached approximately 10 ºC. After the tungsten had fully reacted, the resulting peroxotungstic acid solution was clear and colorless or tinted slightly yellow. The peroxotungstic acid was heated to 55 ºC overnight with a condenser attached. Solvent was removed by rotary evaporation at 40 ºC resulting in a yellow powder of APTA; two liquid nitrogen traps should be employed as acetic acid is highly volatile. APTA was dissolved in 50 mL of methanol overnight and removed by rotary evaporation at 40 ºC resulting in the final product of APTA. For infiltration into a colloidal crystal the powder was dissolved in a

H_2O:methanol mixture (4:1 vol:vol). The FT–IR spectrum of the APTA product was consistent with the published spectrum.[94]

A note on the scale up and scale down of the two APTA syntheses. Scale down is easily achieved; the only factor to consider is that the flask size must be large enough to provide sufficient cooling surface area to volume. On scale up, the same factor of flask size needs to be considered, as well as the period of time over which the tungsten powder is added. If the amount of tungsten added to the flask exceeds 2–3 g of tungsten over 5 minutes, there is a greater probability that the reaction will heat too quickly for the cooling bath to maintain a low temperature. At this point the reaction becomes very rapid, exothermic and evolves gas, thus resulting in the explosion of the solution from the flask. If the tungsten amount is large, it is recommended that the time for addition of each 2–3 g be extended as well.

3.2.3. Preparation of acetylated peroxomolybdic acid (APMoA)

The APMoA synthesis was adapted from the APTA2 synthesis. In a 250 mL round bottom flask, 60 mL of 30 wt% H_2O_2 were combined with 60 mL of glacial acetic acid and cooled to 0 ºC with stirring. Molybdenum powder (2.5 g) was added to the cooled solution in small aliquots over a period of 10 minutes. Caution: cooling was important at this stage, because the reaction of molybdenum and H_2O_2 was exothermic and would occur too rapidly at room temperature. When all molybdenum had been added, the ice bath was allowed to warm up to room temperature. The molybdenum remained unreacted

until the temperature reached approximately 10 ºC. After the molybdenum had fully reacted, the resulting peroxomolybdic acid solution was clear and tinted orange. The peroxomolybdic acid was heated to 55 ºC overnight with a condenser attached. Solvent was removed by rotary evaporation at 35 ºC resulting in a yellow powder of APMoA; two liquid nitrogen traps should be employed as acetic acid is highly volatile. APMoA was dissolved in 50 mL of methanol overnight and removed by rotary evaporation at 35 ºC resulting in the final product of APMoA. For infiltration into a colloidal crystal the powder was dissolved in H_2O.

3.2.4. Preparation of colloidal crystal templates and infiltration techniques

Information on the formation of PMMA colloidal crystals as templates and infiltration techniques can be found in Appendices A and B respectively. Precursor solutions for WCl_6 varied from 0.5-3 M. Tungsten(V) ethoxide was infiltrated neat or as a 1 M solution in ethanol. Tungstic acid and peroxotungstic acid solutions were infiltrated in 0.5 M solutions. APTA1 was employed as a 2-3 M solution. APTA2, AMT, APMoA and AMo were infiltrated as 3 M solutions.

3.2.5. Synthesis of 3DOM metallic photonic crystals

For template removal and metal formation, the infiltrated templates were heated in a tube furnace under an atmosphere of either H_2 or forming gas (10% H_2: 90% N_2) flowing over the sample at a rate of 0.5 L/min. Samples were heated at a rate of 5 ºC/min to temperatures ranging from 400–800 ºC for 1–4 h. Each combustion boat was filled with

up to one full layer of monolithic colloidal crystal composite material for reduction. The layer of material was approximately 5 mm thick.

3.2.6. Characterization

Samples were characterized by SEM, powder XRD and UV–vis. Additional information on these techniques can be found in Appendix C.

3.3. Results and Discussion

3.3.1. Preparation of 3DOM tungsten from solution precursors

Tungsten(VI) chloride, tungsten(V) ethoxide, tungstic acid, peroxotungstic acid, ammonium metatungstate hydrate (AMT) and an acetylated peroxotungstic acid (APTA) were considered as precursors for liquid infiltration. However, not all of these were viable for creating periodic macroporous structures. Tungstic acid and peroxotungstic acid were only sparingly soluble in mixtures of methanol and water, a solvent combination which usually benefits wetting and infiltration of PMMA colloidal crystal templates. With these precursors, little or no porous product was obtained after reduction and template removal. 3DOM materials could, however, be produced when tungsten(VI) chloride, tungsten(V) ethoxide, AMT or APTA precursors were used. Products from these syntheses will be discussed further below.

3.3.2. Preparation of 3DOM W granules from WCl_6 and $W(OEt)_5$ solution precursors

Tungsten powders with typical grain sizes in the range from 10–100 nm can be prepared by reduction of WCl_6 in hydrogen.[96] Small grains in this size regime are necessary to form inverse opal skeletons with sufficient order for photonic crystal applications. Therefore, WCl_6 was examined as a precursor for liquid phase infiltration of colloidal crystals. With PMMA colloidal crystal templates, a methanol/HCl solvent mixture was suitable to keep WCl_6 in solution and to wet and infiltrate the template. The infiltrated and dried samples were heated in hydrogen at various temperatures. Figure 3.1 shows powder XRD patterns of the resulting materials. At 400 ºC, the product consisted mostly of a mixture of WO_x or H_yWO_x phases. At higher temperatures between 500 and 800 ºC, the major phase consisted of bcc tungsten (PDF#04–0806). Based on the line broadening of reflections, the average grain sizes increased from 4.6 to 6.0, 15.1 and 18.1 nm for samples reduced at 500, 600, 700 and 800 ºC, respectively. Even though the tungsten grains were smallest at 500 ºC, the templated macroporosity was minimal for this sample. After this observation, reduction times were shortened from 4 h to 1 h for reactions above 500 ºC. With the shorter reduction time, the sample prepared at 600 ºC contained some tungsten carbide and tungsten oxide as minor impurities, but these were no longer present at 700 or 800 ºC. A reduction temperature of 800 ºC was therefore chosen for subsequent samples. All these products were macroporous and composed of relatively thick spherical shells, many of which were interconnected by small windows. The sample reduced in hydrogen at 800 ºC will be discussed in more detail later. The products prepared by this

method were granular, with typical pieces tens or hundreds of micrometers in length. Some granules contained a non–porous surface crust, which resulted from excess precursor solution. The surface crust could be avoided by employing vacuum infiltration and removal of any non–infiltrated precursor before reduction, a method that was employed for samples based on $W(OEt)_5$ and APTA precursors.

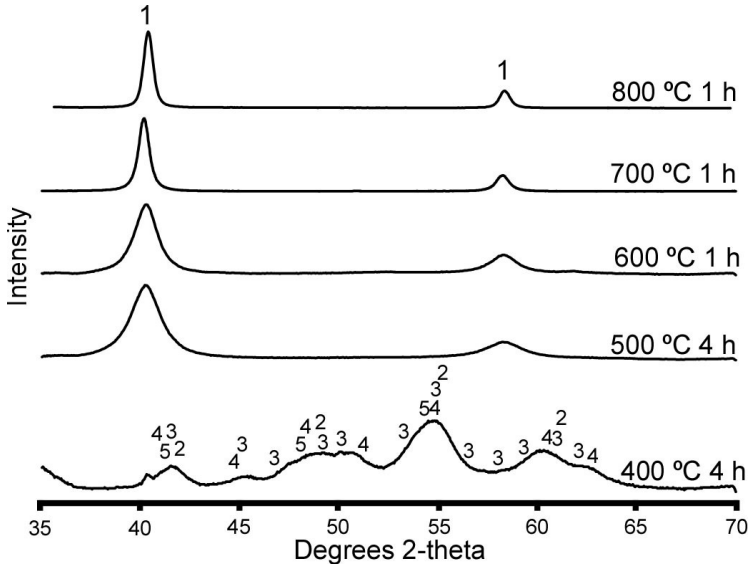

Figure 3.1. Powder XRD patterns of 3DOM samples prepared from a WCl_6 precursor dissolved in methanol/HCl and heated in hydrogen at the indicated temperatures and for the indicated times. A WO_x phase was observed only at the lowest temperature. Under all other conditions, tungsten phases were obtained. (1) PDF#04-0806 W. (2) PDF#41-0905 WO_3. (3) PDF#20-0483$H_{0.23}WO_3$. (4) PDF#18-1417$WO_{2.90}$. (5) PDF#42-1260 $H_{0.23}WO_3$.

An alternate precursor, $W(OEt)_5$, is a liquid at room temperature. Using vacuum infiltration, this precursor could penetrate PMMA colloidal crystals, both as a 1 M solution in methanol or as a neat liquid. After reduction in hydrogen at 800 ºC for 1 h, reasonably well ordered macroporous tungsten structures were obtained, but like the

WCl_6–derived samples, they were granular. Powder XRD patterns of the products, corresponding to a pure tungsten phase, are shown in Figure 3.2.

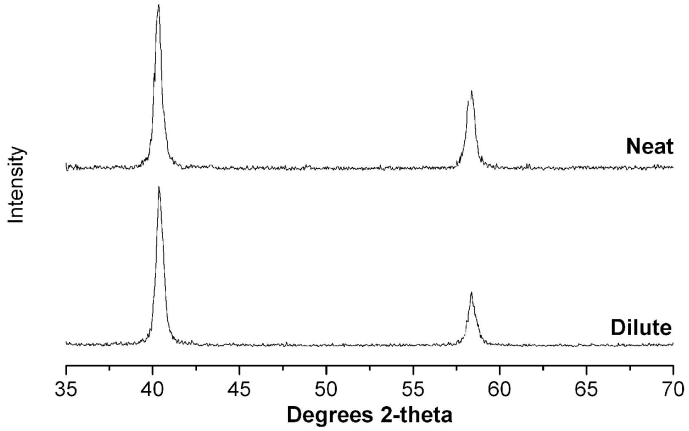

Figure 3.2. Powder XRD patterns of 3DOM tungsten samples prepared from a $W(OEt)_5$ precursor either diluted to 1 M in ethanol or neat and heated in hydrogen at the 800 ºC for 1 h. For both concentrations tungsten phases were obtained.

3.3.3. Preparation of 3DOM tungsten monoliths from APTA precursors

Monolithic 3DOM tungsten pieces large enough for use as a filament in a thermal emission source could be prepared with solutions of APTA. The solubility of peroxotungstic acid in methanol or H_2O:methanol mixtures can be enhanced by acetylation.[94] APTA, which is synthesized by direct reaction of tungsten metal powder with hydrogen peroxide and acetic acid, possesses a low degree of polymerization and high chemical stability.[94] A H_2O:methanol solution of APTA could therefore penetrate a PMMA colloidal crystal without premature precipitation, ensuring uniform access throughout the template. Although APTA can be used for depositing tungsten oxide–based electrochromic films, it can be converted to tungsten by reduction in hydrogen.

Within a PMMA template, a bcc tungsten phase (PDF# 04–0806) was obtained at 800 ºC after exposure to either pure hydrogen (all M samples) or forming gas (10% H_2: 90% N_2) (low M samples only) for 1 h. When forming gas was used to reduce a 2 M APTA1 sample, a tungsten carbide (W_2C) phase (PDF# 20–1315) was obtained at 800 ºC. The corresponding powder XRD patterns are shown in Figure 3.3a and b. Although two different APTA1 concentrations and atmospheres were used, the average grain sizes of tungsten in the 3DOM skeleton were similar, based on XRD line broadening, 18.8 ± 0.2 nm for 1 M APTA1 in forming gas and 24.3 ± 0.1 nm for 2 M APTA1 in hydrogen. The sample prepared with the lower precursor concentration consisted of black pieces several hundred micrometer in size. Even larger monolithic pieces were obtained with 2 M APTA1. These pieces had typical dimensions of 0.5 × 0.5 × 0.2 cm (see Figure 3.4). The surfaces of the monoliths appeared opalescent blue. The 3DOM tungsten monoliths were robust enough to be handled and a moderate pressure could be applied to the pieces before significant destruction of the piece occurred. For the best monoliths, the PMMA template needed to be pre–annealed to avoid separation of spheres and vacuum infiltration had to be employed.

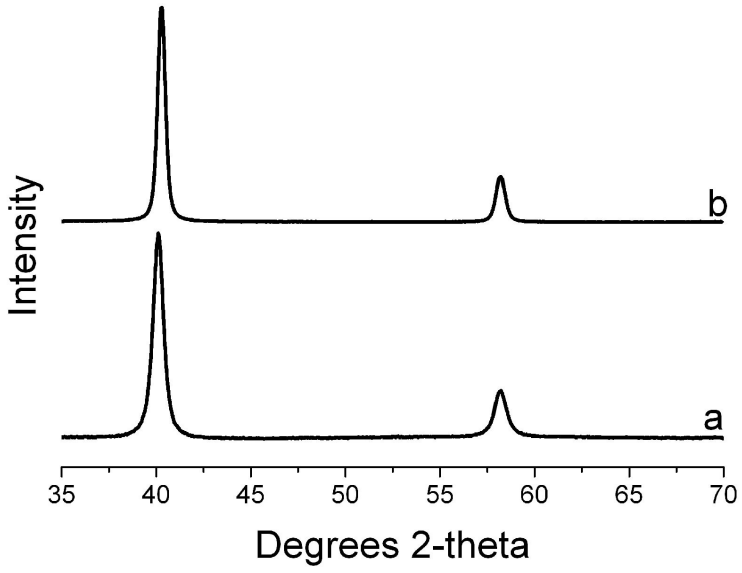

Figure 3.3. Powder XRD patterns of 3DOM tungsten samples prepared from the APTA1 precursor templated in PMMA colloidal crystals. (a) 1 M APTA1, reduced in forming gas. (b) 2 M APTA1, reduced in hydrogen.

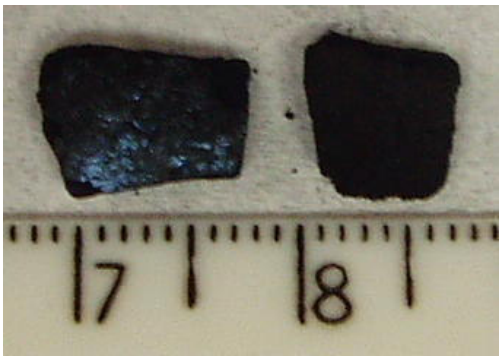

Figure 3.4. Photograph of 3DOM tungsten monoliths produced from a 2 M APTA1 precursor solution. The sample produces an opalescent blue color on the top surface.

While the APTA1 precursor produced the desired 3DOM tungsten monoliths, it had one major flaw: it was difficult to reproduce the precursor concentration consistently from batch to batch. Furthermore, the precursor solution was difficult to work with as the

solution would not fully dissolve in the solution and required filtration before infiltration of the PMMA template. APTA2 was an improved precursor as the final product fully dissolved even at concentrations as high as 3 M. The improved solubility of APTA2 was achieved by lowering the temperature during the purification steps. By lowering the temperature to 40 ºC the APTA2 powder produced was of a higher quality and not baked onto the side of the flask, but if the temperature was lowered too much the APTA2 took on the same qualities as the APTA1 product. Using 3 M APTA2 as a precursor, it was possible to prepare well formed 3DOM tungsten monoliths (Figure 3.5 a) composed of the bcc tungsten phase (PDF# 04–0806). The average grain sizes for tungsten in the corresponding 3DOM skeleton of the APTA2 sample were 19.8 ± 0.1 nm based on XRD grain broadening. 3DOM tungsten samples produced using 540 ± 9 nm PMMA sphere templates contained 328 ± 21 nm voids with 129 ± 12 nm window diameters and wall thicknesses of ca. 39 ± 5 nm (Figure 3.5 c).

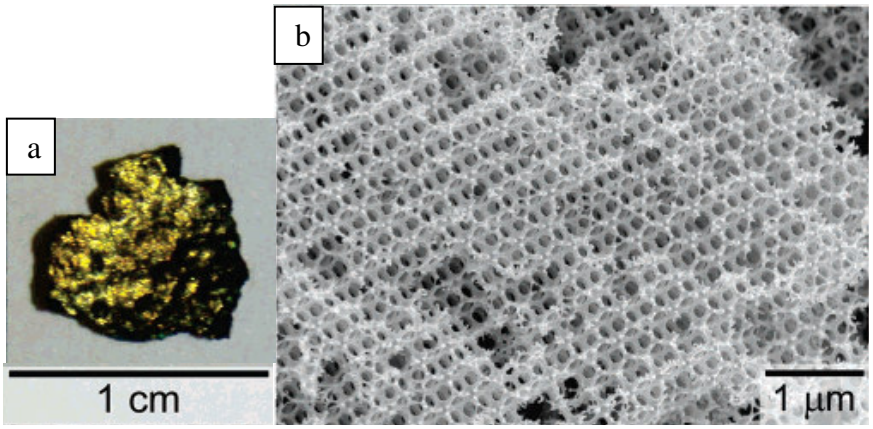

Figure 3.5. (a) Photograph of a 3DOM tungsten monolith prepared from APTA2. (b) SEM image of 3DOM tungsten prepared from APTA2.

3.3.4. Preparation of 3DOM tungsten monoliths from AMT precursors

An alternative to the APTA precursor was the ammonium metatungstate hydrate (AMT) precursor. AMT produced monoliths (Figure 3.6 a) similar to those of APTA but did not produce a nanoporous structure that was as smooth as the APTA precursor discussed above. The benefit of using AMT over APTA, however comes from the known consistent precursor formula that allows for exact reproducibility of precursor concentrations. The ability to reproduce precursor concentrations was particularly important for the study of grain coarsening in a subsequent chapter. After reduction in a pure hydrogen atmosphere, a sample produced from AMT had a bcc tungsten phase (PDF# 04–0806) as determined by XRD. If a 540 ± 9 nm PMMA sphere template was used, a 3 M AMT precursor produced a 3DOM skeleton with 363 ± 25 nm pores, 142 ± 14 nm wide windows and 48 ± 8 nm thick walls (measurement taken from the center of the strut) (Figure 3.6 b).

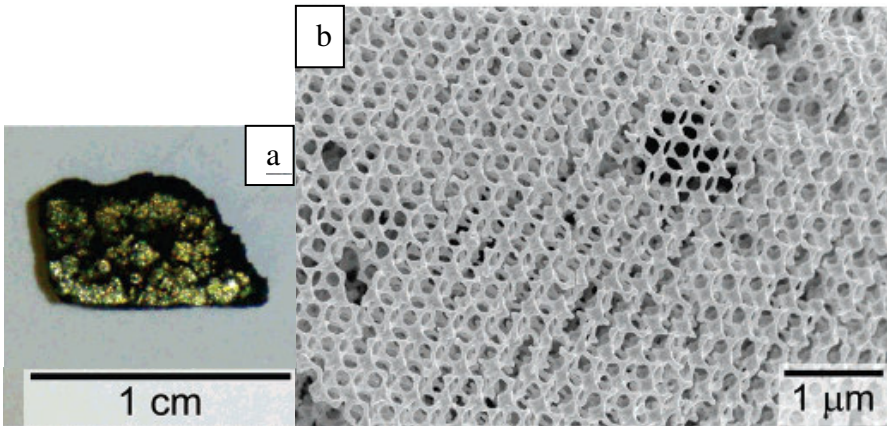

Figure 3.6. (a) Photograph of a 3DOM tungsten monolith prepared from AMT. (b) SEM image of 3DOM tungsten prepared from AMT.

3.3.5. Influence of synthesis parameters on filling fraction, wall thickness and pore window sizes

The filling fraction of tungsten in an inverted opal structure (i.e., the volume of tungsten relative to the complete volume of the porous structure), the thickness of walls in the tungsten skeleton and the size of windows connecting spherical voids can all influence the optical properties of the photonic bandgap structures. Changes in any of these parameters result in shifts of optical stop bands. Furthermore, the transmission properties of a metallic photonic crystal are modified by these structural parameters. Transmission can be enhanced compared to nonporous films.[97] However, the transmission properties in three–dimensional structures depend on the material filling fraction.[97] In this study, we observed distinct differences in structural parameters depending on the precursor ($W(CO)_6$, WCl_6, $W(OEt)_5$, APTA, AMT). Figure 3.7 illustrates these effects. One difference arises from the ability of a precursor to wet or tightly coat a certain template. With strong wetting, one observes surface–templated structures, such as those shown in Figure 3.7 a. This material was prepared by CVD of $W(CO)_6$ on a silica template.[1] Here the walls are highly spherical, thin and touching only at a small intersecting area. Although interconnected through some small windows, the spheres are relatively closed. The other extreme, a highly open volume–templated structure can be seen in Figure 3.7 f. The corresponding material was prepared by solution synthesis employing APTA in a mixed solvent which could penetrate the interstitial spaces in the PMMA sphere array, but apparently did not penetrate individual PMMA spheres. As a result, the skeleton is

[1] 3DOM tungsten synthesized by CVD of $W(CO)_6$ on silica spheres was provided by courtesy of Dr. Sangjin Han.

more stick–like and only outlines the original template spheres. Connecting windows are much larger than in the surface–templated structure. Various mixtures of surface and volume templating were observed under other reaction conditions. For example, the inverse opal prepared using a WCl_6 solution and PMMA had relatively thick walls, which were not quite as smooth as those from CVD. However, except at top surfaces (inset), the voids appeared to be more interconnected than in the CVD sample (Figure 3.7 b). A similar structure was produced with 1 M $W(OEt)_5$ in methanol (Figure 3.7 c). In contrast, with neat liquid $W(OEt)_5$ as a precursor, only very few closed shells were observed on the surface. Most of the product was open with relatively large interconnecting windows, as shown in the SEM image in Figure 3.7 d. Even larger windows could be obtained using the APTA precursor. At a 1 M APTA1 concentration, SEM images (e.g., Figure 3.7 e) provided evidence that insufficient precursor was available in certain parts of the template. In those regions, thin web–like structures surrounded the macropores. Other regions were more fully developed. When the precursor concentrations of APTA1, APTA2 and AMT were 2–3 M, most of the resulting 3DOM tungsten structure was well ordered and composed of a uniform skeleton with the largest interconnecting windows (Figure 3.7 f, 3.5 b, 3.5 b respectively). The resulting monolithic pieces were strong enough to be used as filaments for resistive heating. Comparison of the two samples with different APTA1 concentrations (Figures 3.7 e and f) shows that variations in the solution precursor concentration allow some control over wall thicknesses, similar to changes in the amount of CVD precursor in a fixed reactor volume.

The photonic properties of the APTA2 and AMT samples can be compared as both monoliths were of similar size. The intensity of the stop bands produced by the monoliths changes depending on the smoothness of the walls and openness of the structure. As both samples have similarly open structures on the basis of SEM images, the smoothness seems to be the greatest factor in the intensity of the stop bands. In Figure 3.8, the UV–vis reflectance spectra of the APTA sample (circles) had a far more intense stop band compared to the AMT (squares). This correlates well with observations from the SEM images that the AMT structure appeared to contain rougher walls which correlated to a decreased intensity in the stop band. Figure 3.8 also displays computational data for the theoretical reflectance spectrum calculated from the structure parameters of the 3DOM tungsten sample produced from APTA (solid line).[2] The intensities of the two lines match well, demonstrating that the materials produced from the APTA precursor were sufficiently open to achieve a photonic stop band consistent with those of a highly open structure as predicted by computational studies.[16] The peak maxima for the predicted and actual materials were not at the same wavelength which was attributed to deviations in sample angle acquisition.

[2] Theoretical calculations performed by Dr. Sang Eon Han.(16) Han, S. E.; Stein, A.; Norris, D. J. *Phys. Rev. Lett.* **2007**, *99*, 053906/1-053906/4.

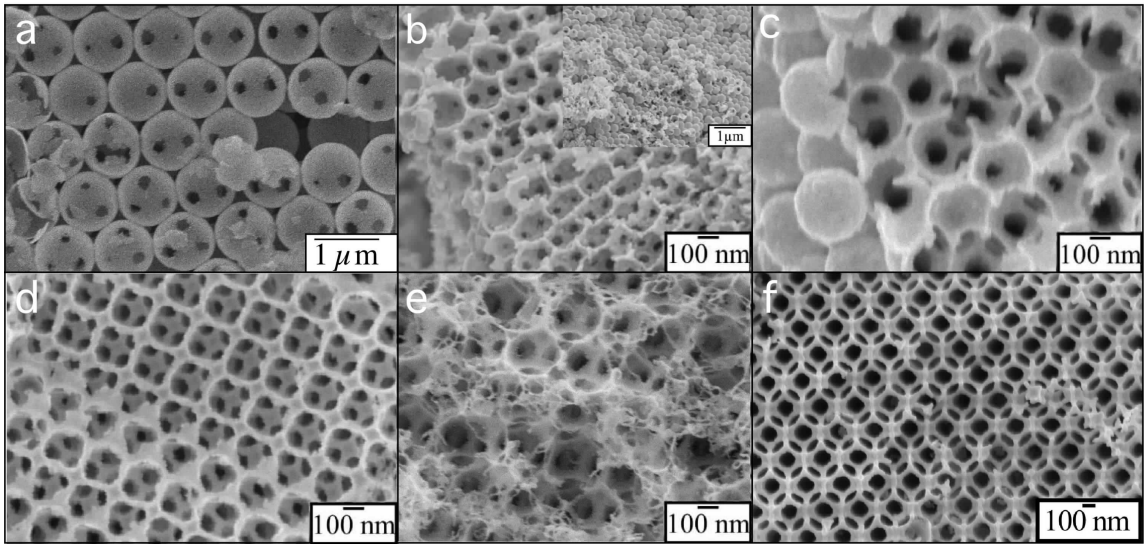

Figure 3.7. SEM images of 3DOM tungsten samples prepared by using various methods and precursors. (a) CVD synthesis using 0.2 g $W(CO)_6$ resulted in surface templating and produced a collection of hollow spheres with small windows after template removal. (b) Solution synthesis using WCl_6 in methanol/HCl also resulted in mostly surface templating. The inset shows that connected spheres were obtained, but they occupied a larger volume fraction than in (a). (c) Solution synthesis with 1 M $W(OEt)_5$ in methanol produced similar results as with WCl_6. Closed spheres were observed only on the sample surface and partly interconnected voids indicated good template–wetting with a large contribution of surface templating. (d) In a sample prepared from neat $W(OEt)_5$, pore openings were larger and fewer closed spheres were noted. (e) Solution synthesis with 1 M APTA1 in H_2O/methanol led to mostly volume templating. Relative window sizes compared to void diameters were now larger. However, at this concentration there was not enough precursor material in all interstices of the template to fill it completely. As a result some skeletal areas appeared web–like. (f) Solution synthesis with 2 M APTA1 in H_2O/methanol produced the most open structure with the largest windows mostly by volume templating. At this concentration, the skeletal thickness was much more uniform than in (e). The sample in (a) was prepared with a silica colloidal crystal template, all other samples with PMMA colloidal crystal templates. All samples were reduced at 800 ºC for 1 h in H_2, except for the sample in (e), which was reduced in forming gas.

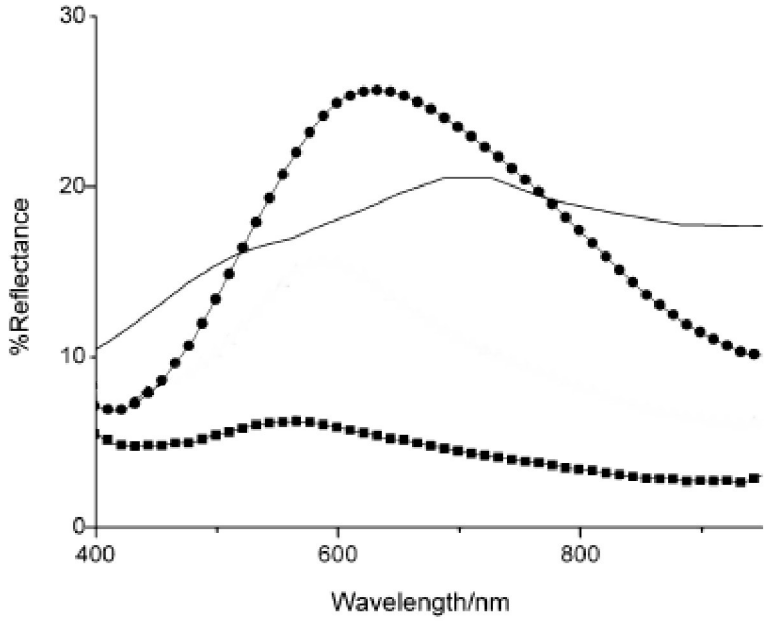

Figure 3.8. UV–vis reflectance spectra taken from the top surface of the monoliths depicted in Figure 3.5 and Figure 3.6 normal to the (111) planes. Circles correspond to data for the 3DOM tungsten sample prepared from APTA2 and squares to the sample prepared from AMT. The thin line is a simulated reflectance spectrum for 3DOM tungsten with structural parameters corresponding to the sample prepared from APTA2.

3.3.6. Preparation of 3DOM molybdenum precursors

Both ammonium molybdate tetrahydrate (AMo) and acetylated peroxomolybdic acid (APMoA) were considered as precursors for liquid infiltration of PMMA colloidal crystal templates. To obtain a 3 M clear solution of the AMo precursor, H_2O had to be used as the solvent. With pure ethanol or a H_2O:methanol (4:1 vol:vol) mixture as the solvent for the AMo precursor, a 3 M clear solution could not be obtained and large amounts of undissolved AMo were observed even after vigorous stirring and with slightly elevated temperatures. For the APMoA precursor, great care should be taken during solvent

removal steps during the synthesis. High temperatures or too long solvent removal times (2.5 h or more) created an APMoA precursor that formed a glassy film and was difficult to remove from the reaction vessel. The APMoA precursor formed a slightly cloudy solution in the H_2O:methanol (4:1 vol:vol) mixture which indicated that a small portion of APMoA was not dissolved. In ethanol, the APMoA precursor dissolved rapidly and completely to produce a clear 3 M solution. Both AMo and APMoA were employed to produce 3DOM molybdenum using all solvents discussed above. The results of those experiments are discussed below.

3.3.7. 3DOM molybdenum materials

3DOM molybdenum materials can be obtained from both APMoA and AMo. When a solvent mixture of H_2O:methanol (4:1 vol:vol) was used for APMoA, granules were formed that had an overall size of 10s of μm. The structure of the samples was highly ordered as seen in most 3DOM materials but it also contained extended, non-templated void volumes that may indicate incomplete penetration of the template interstitial areas by the precursor (Figure 3.9 a). The incomplete penetration of the template can be attributed to an increase in hydrodynamic volume of the molybdenum precursor as discussed below. When the solvent was changed to ethanol for the APMoA precursor, the 3DOM material produced appeared to be more fully connected than the previous sample (Figure 3.9 b). However, partial monoliths were observed with the latter sample (Figure 3.9 c) compared to granular materials. Partial monoliths were monolithic samples with hollow centers that formed a bowl shape. The partial monolith instead of the granular

result could be to some extent attributed to the ethanol fully dissolving the APMoA. The solvent mixture was slightly cloudy even after heating, possibly leading to incomplete infiltration and the formation of granules rather than a partial monolithic sample. However, after infiltration, both samples maintained a composite template material that appeared to be fully infiltrated. In the previous tungsten samples above, fully infiltrated templates produced monolithic samples. This was not the case for the APMoA samples. It was believed that the APMoA samples produce highly conjugated polyoxometalates in the presence of alcohol that can grow up to a few 10s of nm in size thus increasing their hydrodynamic volume.[98] Furthermore, polyoxometalates form rapidly for molybdenum and take days for tungsten which accounts for the differences in the monolithic structure.[99] As the hydrodynamic volume of the polyoxometalates increases, the colloidal crystal acts like a size exclusion chromatography column preventing the larger molybdenum containing particles to infiltrate deeper into the template. Thus the mixed solvent precursor possibly contained larger particles than the sample in ethanol only, producing a granular material rather than a partial or full monolith. It is also probable that the pure ethanol solvent wetted the PMMA better resulting in the partial monolith. Partial monoliths were formed as the outside layers of the colloidal crystal were clogged with material, preventing a sufficient amount to reach the middle regions of the monolith and thus creating a hollow void (like a bowl) after reduction (Figure 3.9 c). Even the bottom of the monolith was extremely thin as the template was in contact with the bottom of the dish and did not allow for the precursor solution to easily flow into the monolith from that direction.

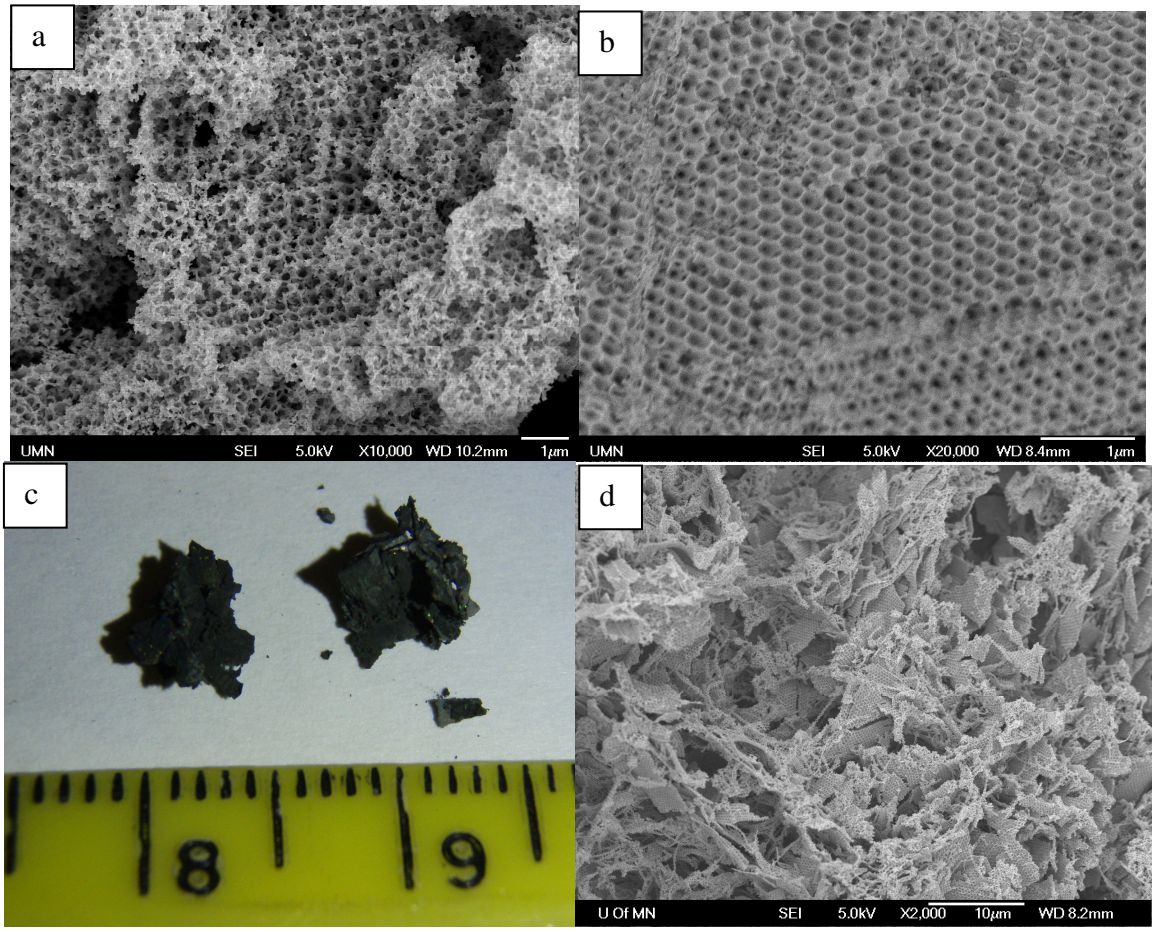

Figure 3.9. (a) SEM image of 3DOM molybdenum granules fabricated from a 3 M solution of APMoA in a H_2O:methanol (4:1 vol:vol) mixture. (b) SEM images of 3DOM molybdenum partial monoliths from a 3 M precursor solution of APMoA in EtOH. (c) Photograph of a partial monolith of the sample produced from APMoA (cm scale). (d) SEM images of 3DOM molybdenum partial monolith produced from a 3 M solution of AMo in H_2O.

The AMo precursor was only able to be fully dissolved in H_20 and produced similar results to the APMoA precursor. With a concentration of 3 M, the AMo precursor produced a composite monolith that appeared to be fully infiltrated after permeation of

the precursor but produced a partial monolith similar in shape to the APMoA partial monolith. The ordered structure however was quite different as the AMo contained many void regions next to areas of high periodicity (Figure 3.8 d). This result was consistent with the hypothesis that highly conjugated polyoxometalates increase their hydrodynamic volume and will be retained closer to the edges of the template structure during infiltration. In addition, the ammonium causes polyoxometalates to form faster[98] which could be the cause for the sheet like structures shown in Figure 3.8 d.

3.4. Conclusion

3DOM molybdenum and 3DOM tungsten could be produced form a variety of metal-containing precursors. The materials produced from molybdenum precursors range from granules (APMoA) to partial monolithic structures (APMoA, AMo). The nanostructure of these materials was well ordered over the portions that were infiltrated. However the precursors did not infiltrate evenly throughout the structures even though the template appeared uniform in color which for other precursors indicated a full infiltration of the template. The partial filling of the structure could be attributed to the formation of polyoxometalates with possible aggregate sizes in the 10s of nm as molybdenum is known to form these in the presence of alcohol and ammonium containing solutions.[98] The polyoxometalate most likely clogged the interstitial areas nearest to the template surface and prevented higher concentrations of precursor to diffuse throughout the entire template causing the formation of partial monoliths. The polyoxometalate formation prevented the production of fully formed monoliths. The production of 3DOM

molybdenum using a colloidal crystal thin film as the template may be an alternative to producing reproducible uniformly sized samples as the monolithic templates.

Several precursors were identified that can be used to prepare granules or monoliths of 3DOM tungsten. Pieces of 3DOM tungsten, with larger volumes and more sample material than similarly nano-structured samples prepared from CVD[15], were prepared using liquid infiltration methods with PMMA opal templates. The type of templating (surface templating vs. volume templating) varied with precursor and depended on the ability of the precursor to effectively wet the template. Based on trends of increasing window size and decreasing skeletal curvature, the relative contribution of volume templating increased approximately in the order $WCl_6 \approx W(OEt)_5$ in methanol < neat $W(OEt)_5$ < AMT ≈ APTA1&2. Wetting can also be a function of the surface groups on a polymer template. In this study, PMMA spheres prepared with an azo initiator were employed for all precursors except AMT and APTA2 where a persulfate initiator was employed. These spheres carry a small positive or negative surface charge, respectively, which can affect the type of templating depending on the precursor charge.

While most samples prepared by liquid infiltration were granular, larger monolithic pieces several millimeters on each side could be prepared from APTA and AMT precursors. Structural optimization required the use of an annealed polymer template, vacuum application of the precursor solution for complete infiltration, keeping the precursor concentration sufficiently high for formation of a well–developed skeleton,

decreasing the precursor/template interaction by addition of water to the alcoholic solvent, and use of hydrogen at a reduction temperature that led to formation of a pure tungsten phase without inducing too much grain growth. Having determined the dependence of tungsten photonic crystal structures on synthesis parameters, we are now able to prepare metallic photonic crystals that are suitable to study structural effects at varying temperatures. Even though the 3DOM tungsten structures obtained by colloidal crystal templating contain some structural defects, the primary requirement to observe the desired photonic effects is to have a 3D metallic network. Therefore, slight imperfections in the overall broader structure that maintain the unit cell over three or more periods are not expected to have a detrimental effect.[16] The wet chemical methods provide a low cost alternative to expensive nanolithographic methods for the fabrication of three–dimensional periodic metallic structures.

Chapter 4

Investigation of 3DOM Metallic Photonic Crystals under Thermal Treatment and the Effects of Alloying

Outline

4.1. Introduction

3DOM tungsten materials described in the previous chapter exhibited highly open structures and monolithic forms.[92,93] The monolithic nature of these materials makes them a good candidate for use as a light bulb filament as the pieces are large and robust enough to be placed in a testing device. 3DOM tungsten however does not contain any dopants or alloys that have been shown to be beneficial towards reducing grain growth in other materials.[23] For example, non-sag tungsten wires used in incandescent light bulbs today have potassium, silicon and aluminum incorporated as dopants.[23,100] However, these dopants are volatile at higher temperatures and are actually contained in the structure between grains. This is not possible in the 3DOM W structures as the walls are only 1 or 2 grains thick and each grain is about 20 nm in size. As well, 3DOM tungsten materials produced in earlier studies undergo grain coarsening and needle formation when resistively heated or heated radiatively in an inert atmosphere as described below.[93] The needle formation has been known to be suppressed by the incorporation of Mo into the W structure.[101] This chapter discusses the use of a Mo alloy with the 3DOM W materials and its effects on grain coarsening. Two distinct precursors are employed to form the 3DOM W/Mo alloys, a combination of the acetylated precursors specified in the previous chapter and a combination of the ammonium metatungstate and molybdate precursors. In the next chapter the effect of the alloy on grain coarsening will be studied.

4.2. Experimental

4.2.1. Materials

The following chemicals were used as–received: molybdenum powder (99.9+%, 1–2 μm), tungsten foil (0.05 mm, 99.9+%) and tungsten powder (monocrystalline, 99.9+%, 0.6–1 μm) from Aldrich Chemical Company; methanol (99.9%) from Fisher Scientific; ammonium metatungstate hydrate (AMT) (≥99.0% as WO_3) from Fluka; ammonium molybdate tetrahydrate (AMo), glacial acetic acid (99.9%) and hydrogen peroxide (30%) from Mallinckrodt Chemicals; ethanol (200 proof, anhydrous) from Pharmco-AAPER and Commercial Alchohols; Ar (high purity grade) and H_2 (industrial grade) from the University of Minnesota, U–Stores. Distilled deionized water produced with a resistivity of 18.2 MΩ–cm was used. N_2 was obtained from the University of Minnesota house system. 3DOM W was prepared as outlined in Chapter 3.

4.2.2. Tungsten/molybdenum precursor preparation (APTA/APMoA)

The alloy precursor synthesis for a combined precursor of acetylated peroxo(tungstic/molybdic) acid (APTA/APMoA) was adapted from the previous two syntheses of acetylated peroxotunstic acid and acetylated peroxomolybdic acid that are described in chapter 3. In a 250 mL round bottom flask, 60 mL of 30 wt% H_2O_2 were combined with 60 mL of glacial acetic acid and cooled to 0 ˚C with stirring. W and Mo powders were added to the cooled solution in small aliquots over a period of 10 minutes. When producing the alloy precursor, no more than 0.028 moles of combined W/Mo power was reacted per 120 mL of hydrogen peroxide/acetic acid solution. Caution:

cooling was important at this stage, because the reaction of W/Mo and H_2O_2 was exothermic and would occur too rapidly at room temperature. When all W/Mo had been added, the ice bath was allowed to warm up to room temperature. The W/Mo remained unreacted until the temperature reached approximately 10 ˚C. After the W/Mo had fully reacted, the resulting peroxoalloy solution was orange (equal W to Mo ratio by weight) or yellow (high W content). The peroxoalloy was heated to 55 ˚C overnight with a condenser attached. Solvent was removed by rotary evaporation at 40 ˚C for solutions with high W content and 35 ˚C for solutions containing equal masses of W to Mo, the solutions resulted in a yellow or orange powder of APTA/APMoA respectively; two liquid nitrogen traps should be employed as acetic acid is highly volatile. APTA/APMoA was dissolved in 50 mL of methanol overnight and removed by rotary evaporation at 40 ˚C for solutions with a high W content and 35 ˚C for solutions solution with a high Mo content resulting in the final product of APTA/APMoA. For infiltration into a colloidal crystal the powder was dissolved in a H_2O:methanol mixture (4:1 vol:vol).

4.2.3. Preparation of colloidal crystal templates and infiltration techniques

Information on the formation of poly(methyl methacrylate) (PMMA) colloidal crystals as templates and infiltration techniques can be found in Appendices A and B respectively. All precursors were added at a 3 M concentration to the templates in H_2O and a H_2O:methanol mixture (4:1 vol:vol).

4.2.4. Synthesis of 3DOM W/Mo alloys

For template removal and metal formation, the infiltrated templates were heated in a tube furnace under an atmosphere of H_2 flowing over the sample at a rate of 0.5 L/min. Samples were heated at a rate of 5 ˚C/min to 800 ˚C for 1 h. Each combustion boat was filled with up to one full layer of monolithic colloidal crystal composite material for reduction. The layer of material was approximately 5 mm thick.

4.2.5. Joule heating

Samples were heated resistively in one of two devices. The first consisted of a glass jar fitted with a rubber stopper to control the atmosphere and insulate the electrical leads. The jar was purged with N_2 overnight and during emission at a rate of 0.5 $L \cdot min^{-1}$ using syringe needles. The second device was manufactured by MDC Vacuum Products.[3] The main body consisted of a UHV 6-way configuration flange assembly using Del-Seal CF fittings. A medium current electrical feed through was used to resistively heat the samples while in the chamber. A CaF_2 window manufactured by Crystran Ltd. was used for sample observation. The UHV assembly was evacuated using a Varian Turbo V-70 pump overnight. After evacuation to 2×10^{-4} torr the chamber was refilled with Ar to 760 torr. The chamber was then evacuated and refilled 2 additional times before emission testing to exclude as much water from the sample atmosphere as possible. In both devices, 3DOM samples were heated resistively by sandwiching the monoliths between

[3] Second joule heating chamber initially designed by Dr. San Eon Han and modified by Dr. Sanjin Han and Nicholas R. Denny.

two sets of W foil pieces to create an electrical contact and providing 10–35 W of power supplied by a Tenma CPX200 Dual 35 V 10 A power supply unit.

4.2.6. Radiative heating

Samples were heated in a quartz tube under flowing N_2 at 0.5 $L \cdot min^{-1}$ with a ramp rate of 10 $^{\circ}C \cdot min^{-1}$ to 500, 800, or 1000 ºC and dwell times of 30 min, 1 h, 2 h or 4 h.

4.2.7. Characterization

Samples were characterized by SEM, powder XRD and ICP-mass spectrometry. Additional information on these techniques can be found in Appendix C.

4.3. Results and discussion

4.3.1. Joule heating of 3DOM W

Because the 3DOM W samples were self-supporting and monolithic in nature with dimensions on the order of millimeters, they could be employed directly as filaments through resistive heating (Joule heating). Thermal emission testing required an inert atmosphere to avoid oxidation of the 3DOM W filaments. Two different set-ups were employed for Joule heating. The first device consisted of a glass vessel with a rubber stopper and feed-throughs for wire connections and sample purging (Figure 4.1). The monoliths were sandwiched between two sets of W foil at each end which also provided the electrical contact.

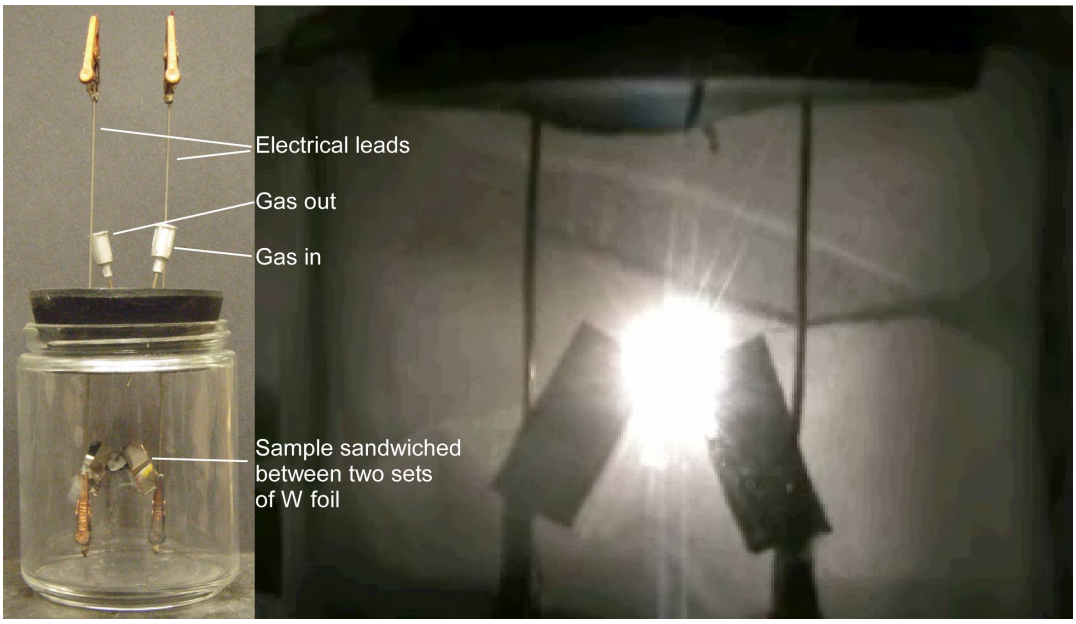

Figure 4.1. Photographs of the first joule heating device. Right photograph of the glowing 3DOM W monolith also shown in Figure 4.2 A.

Although this emission device did not allow for sample evacuation or rigorous exclusion of water in the sample atmosphere, it was useful for rapid qualitative measurements. When a sample of 3DOM W was resistively heated in flowing nitrogen, it began to glow brightly, illuminating the area around the sample. With many samples, emission of light could be maintained over several minutes at powers of 10–35 W. In some samples, the most intense emission wandered throughout the monolithic filament, possibly through cracks and defects in the structure. Figure 4.2 A shows the SEM image of a sample prepared from APTA1 that had emitted light for 15 minutes with an applied power of 35 W. This filament had retained a monolithic shape but was more brittle than before Joule heating. From the SEM image it is clear that the 3DOM structure had been lost for this sample. Instead, relatively large, micrometer-sized tungsten needles were produced in

addition to globular tungsten structures resulting from grain coarsening. Prior to emission, this sample had a structure similar to that found in Figure 3.7 f with an average grain size of 24.3±0.1 nm. After emission the grain size was too large to be determined by XRD line broadening.

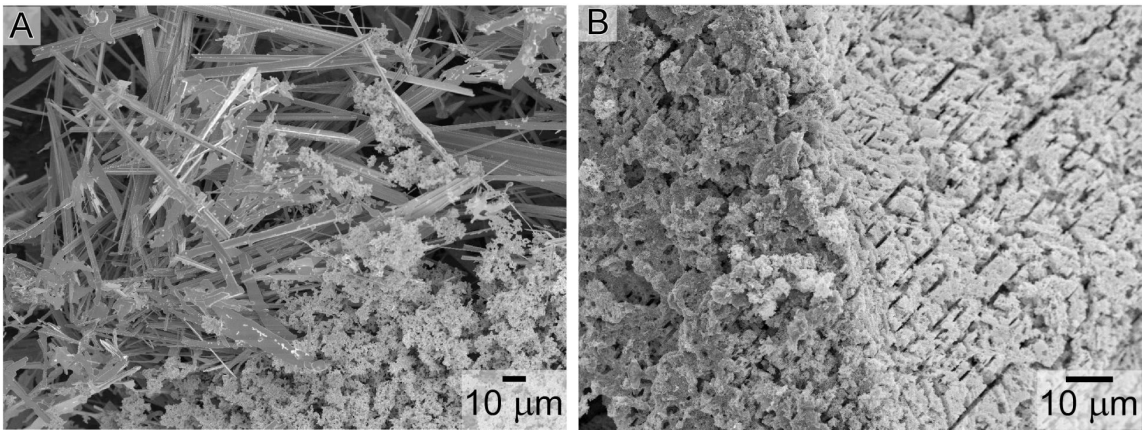

Figure 4.2. Typical SEM images of 3DOM W, prepared from APTA solutions (2.5 M in (A), 3.0 M in (B)), after thermal emission. (A) Product after emission at 35 W for 15 min in the first emission device. (B) Product after emission at 10 W for 5 min in the second emission device.

The needles are a result of chemical vapor transport involving the volatile $WO_2(OH)_2$ phase produced when hot 3DOM W reacted with residual water on its surface or in the device atmosphere (Equation 4.1).[23]

$$W(s) + 4H_2O(g) \Leftrightarrow WO_2(OH)_2(g) + 3H_2(g) \qquad \text{(Equation 4.1)}$$

These observations emphasize the importance of rigorously excluding water vapor from nanostructured tungsten filaments. Subsequent thermal emission studies of 3DOM W samples were therefore carried out in a testing device that could be fully evacuated (Figure 4.3). This device consisted of a metal chamber with ports to provide electrical feed-through, an observation window and atmospheric control.

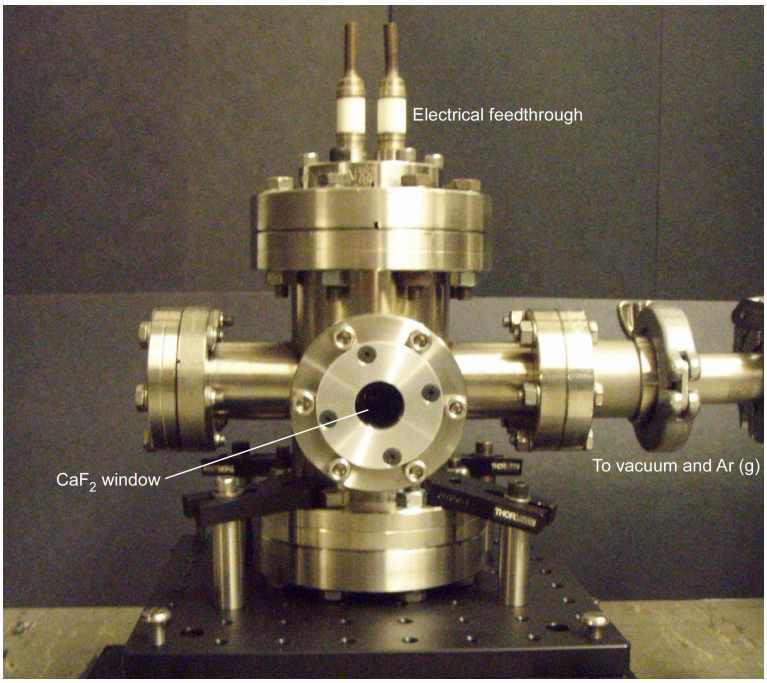

Figure 4.3. Photograph of the second joule heating chamber.

After insertion of the 3DOM W sample, again sandwiched between two sets of tungsten foil, the chamber was evacuated three times to 2×10^{-4} torr and refilled with argon each time. The sample was then resistively heated. Emission was not always uniform across the sample and the brightest spots of emission often occurred between the tungsten foil contacts on either side of the sample. Figure 4.2 B shows an SEM image of the 3DOM W

product (from APTA2) after emission with an applied power of 10 W for 5 min. The lower power and shorter heating time were chosen to mitigate effects of grain coarsening. After emission the monolithic nature of this sample was maintained but it was significantly more brittle at and near the areas of emission. As seen in Figure 4.2 B, no tungsten needles were present in this sample as a result of excluding water from the system. Nonetheless, extensive grain coarsening was still detected in areas of the sample where the brightest emission had been observed (left half of image). In regions away from these local hot spots, less change in the sample structure was apparent (right half of image).

4.3.2. Radiative heating of 3DOM W

One limitation of Joule heating in these devices was the lack of control over the emission temperature. With additional effects of local hot spots, temperatures throughout the monoliths were not uniform. In order to ensure a more uniform thermal history throughout the samples, and to evaluate the effects of temperature and heating time on grain coarsening and on the structural integrity of 3DOM W, samples were heated radiatively in quartz tubes under flowing nitrogen. Figure 4.4 shows SEM images of a 3DOM W sample prepared from AMT as the precursor before and after radiative heating in nitrogen. 3DOM W prepared from APTA produces identical results when radiatively heated. After heating at 500 °C, no structural change was observed after 30 min (SEM not shown). At 800 °C, significant fractions of the 3DOM structure were maintained after 30 min, although they had fragmented into smaller domains (Figure 4.4 B). Tungsten

needles were observed in this product because water could not be completely excluded from the system, in spite of extensive purging with nitrogen. The structures of samples heated to 800 °C for 1 h (SEM not shown) and 1000 °C for 30 min (Fig. 4.4 C) were less regular and grain coarsening continued, so that after 1 h at 1000 °C little of the original 3DOM structure was retained (Figure 4.4 D). These studies indicated that photonic crystals involving tungsten with features on the order of 10s of nanometers were quite reactive and prone to structural changes at temperatures as low as 800 °C. The high surface-to-volume ratios in these structures facilitated surface reactions, sample evaporation and grain coarsening. Grain growth remained an issue even when water was excluded. A promising solution to these issues was provided by alloy formation with molybdenum.

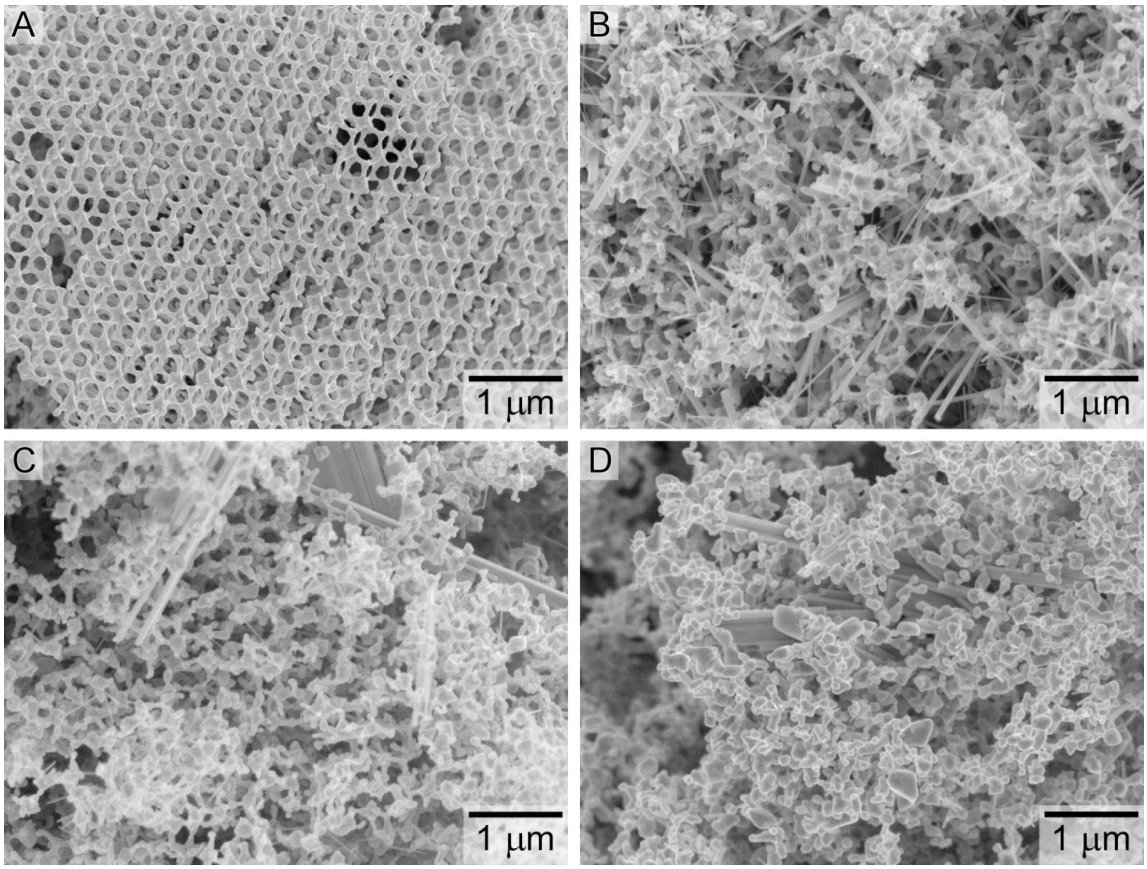

Figure 4.4. SEM images of 3DOM W samples prepared from AMT. (A) Sample before radiative heating. (B) Product after radiative heating in nitrogen flowing at 0.5 $L \cdot min^{-1}$ at 800 °C for 30 min. (C) Product heated at 1000 °C for 30 min. (D) Product heated at 1000 °C for 1 h.

4.3.3. Preparation of 3DOM W/Mo precursors

3DOM W/Mo was produced from precursor solutions of both APTA/APMoA and a mixture of ammonium metatungstate hydrate (AMT) and ammonium molybdate tetrahydrate (AMo). The APTA/APMoA was dissolved in a H_2O:methanol (4:1 vol:vol) mixture and produced a yellow or orange clear solution when dissolved. Both 95:5 and 50:50 wt% W:Mo precursor solutions were investigated using the APTA/APMoA precursor. For mixtures of AMT-AMo, only 95:5 wt% by W:Mo was investigated in a

H_2O:methanol (4:1 vol:vol) mixture and a 3 wt% Mo-containing solution in H_2O. The use of AMT-AMo to produce the alloy structure was adapted from a procedure by Cheetham et al.[102] The aqueous sample of AMT-AMo was clear when used to infiltrate a template. The precursor did not dissolve completely in an H_2O:methanol mixture, even when the mixture was heated. The solution was still employed to infiltrate a template.

4.3.4. 3DOM W/Mo alloy materials

3DOM W/Mo alloy materials can be obtained from AMT-AMo or APTA/APMoA. With a 50:50 wt% of W:Mo, granules 100's of micrometers in size were produced from the APTA/APMoA precursor. The SEM image in Figure 4.5 A revealed a highly ordered structure of the sample and areas depicting a wispy structure. Wispy structures were previously observed in 3DOM W samples (Figure 3.7 E) where low precursor concentrations produced regions of incomplete precursor infiltration. The lower concentration of precursors in these regions may be attributed to polyoxometalate formation. A 50:50 wt% of W:Mo corresponded to an approximately mole ratio of 1:2. With a precursor solution comprised of 2/3rds Mo precursor, there was a significant possibility that highly conjugated polyoxometalates will form. Polyoxometalates of Mo form in the presence of ammonium in solution and form rapidly compared to W. [99] These Mo polyoxometalates can be 10s of nm in size[98] and will have a higher retention in the outer regions of the template, thus lowering the concentration of precursor in regions further from the surface of the template, leading to wispy materials. When the ratio of W:Mo was changed to 95:5 wt% (approximately a 9:1 mole ratio), monolithic materials

were produced. The SEM image in Figure 4.5 B revealed a highly ordered structure that did not contain any appreciable void spaces or wispy structures. It was hypothesized that the low concentration of Mo in the precursor solution prevented the formation of detrimental polyoxometalate structures. By ICP-mass spectrometry analysis, the wt% of Mo in the sample was 4.95%. Monolithic 3DOM W/Mo was also produced using AMT-AMo with solutions at 95:5 wt% W:Mo in a H_2O:methanol mixture and 97:3 wt% solution in H_2O only. The SEM image in Figure 4.5 C shows the high degree of order of samples prepared from a H_2O:methanol mixture which was almost identical to the structure of the sample prepared in an aqueous solution revealed in Figure 4.5 D. The H_2O:methanol mixture contained 2.8 wt% Mo which was far below the theoretical value of 5 wt%. By changing to H_2O as the only solvent, the sample had a wt% of 2.6 for Mo which accounted for far less loss of Mo during the synthesis but still a loss of 14%. The lower than expected Mo content of the AMT-AMo samples was also attributed to the formation of polyoxometalates. Unlike the APTA/APMoA sample, this sample did not employ a precursor that was synthesized with both W and Mo at the same time. When synthesizing a precursor that incorporated both W and Mo at the same time, the precursor probably comprised of small clusters of material that contained both W and Mo. This would then most likely inhibit the production of highly conjugated polyoxometalates as the W precursor does not readily form these.[99] The AMT-AMo sample however contained $(NH_4)_6Mo_7O_{24}•4H_2O$ from the AMo. The AMo was initially slightly conjugated and most likely formed a heterogeneous structure as the solution mixed and polyoxometalates with a higher degree of conjugation formed. As mentioned in chapter 3,

these highly conjugated structures increased their hydrodynamic volume and were unable to fully infiltrate the structure. Thus, a lower Mo content was obtained.

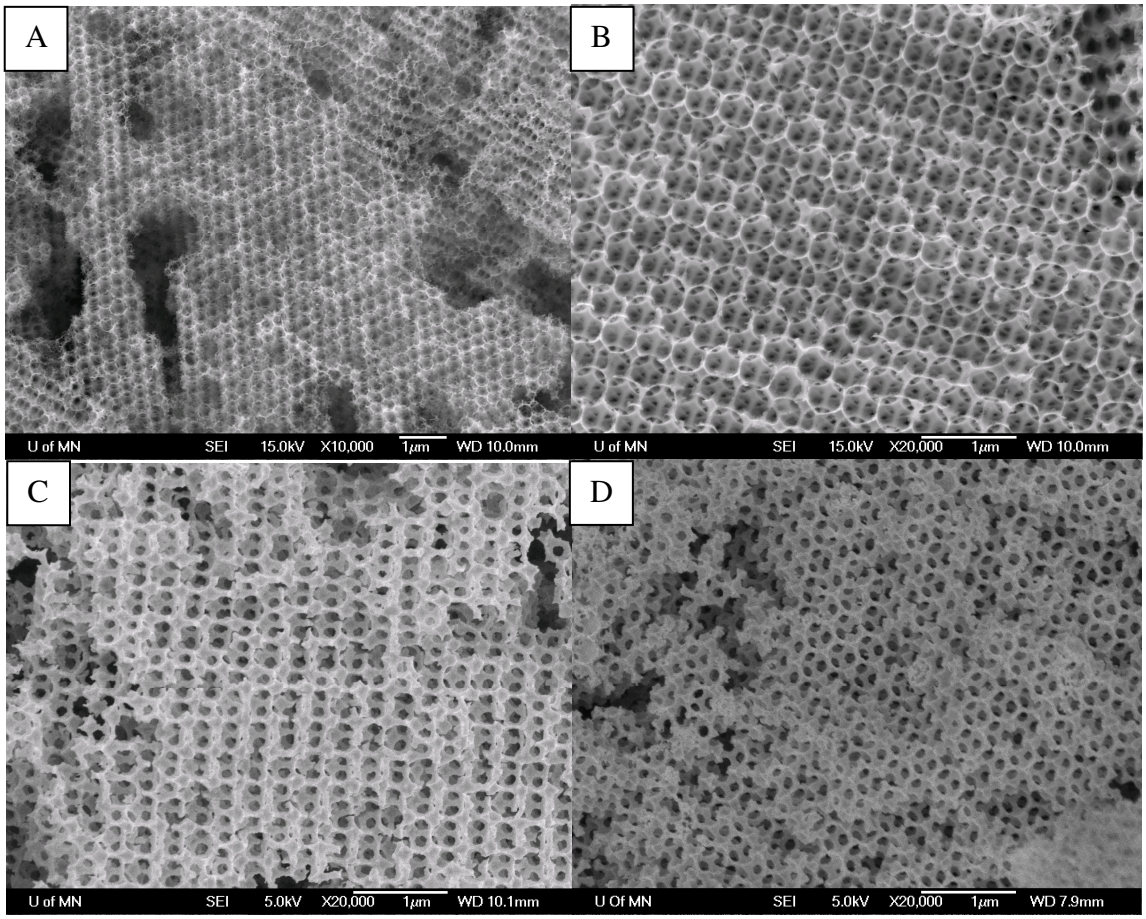

Figure 4.5. SEM images of 3DOM W/Mo alloy samples. (A) Sample with a W:Mo ratio at a 50:50 wt% produced from APTA/APMoA in a H_2O:methanol mixture. (B) Sample with a W:Mo ratio of 95:5 wt% produced from APTA/APMoA in a H_2O:methanol mixture. (C) Sample with with a W:Mo ratio of 95:5 wt% produced from AMT-AMo in a H_2O:methanol mixture. (D) Sample with a W:Mo ratio of 95:5 wt% produced from AMT-AMo in H_2O.

4.3.5. Radiative heating of 3DOM WMo

The effects of radiative heating on 3DOM WMo alloys produced from AMT-AMo are shown in the SEM images of Figure 4.6. It is notable that needles were absent from all samples, except for a few very small needles in the sample heated at 1000 °C for 1 h, indicating that molybdenum does in fact mitigate chemical vapor transport reactions. Furthermore, the 3DOM structure was maintained in these alloys even after heating at 800 °C for 4 h. Grain sizes estimated from XRD line broadening remained approximately constant during this treatment (Table 4.1). Even though samples with both solvent systems were employed for radiative testing, it was believed that the solvent would not change the final product before or after coarsening as the AMT/MoA samples produced similar coarsening results. After heat treatment at 1000 °C for 30 minutes, some sintering was observed, but the change was significantly less than in the molybdenum-free samples. After 1 h at 1000 °C, grain coarsening became significant.

Table 4.1. Average Metal Grain Sizes Before and After Thermal Treatments of 3DOM WMo[4]

Heating temperature	Initial	After 30 min	After 1 h	After 4 h
AMT-AMo 800 °C	27.9±0.2 nm	27.4±0.3 nm	30.9±0.3 nm	29.6±0.2 nm
AMT-AMo 1000 °C	28.7±0.2 nm	41.5±0.3 nm	49.0±0.5 nm	not determined

[4] Grain sizes were determined from line broadening in XRD powder patterns. AMT-AMo samples heated to 800 °C were originally prepared using only H_2O as the solvent, samples heated to 1000 °C were prepared using H_2O:methanol solvent mixtures. Grain sizes could not be determined for 3DOM W samples after radiative heating as the needle structures dominated the line broadening in XRD powder patterns and where over 1 μm.

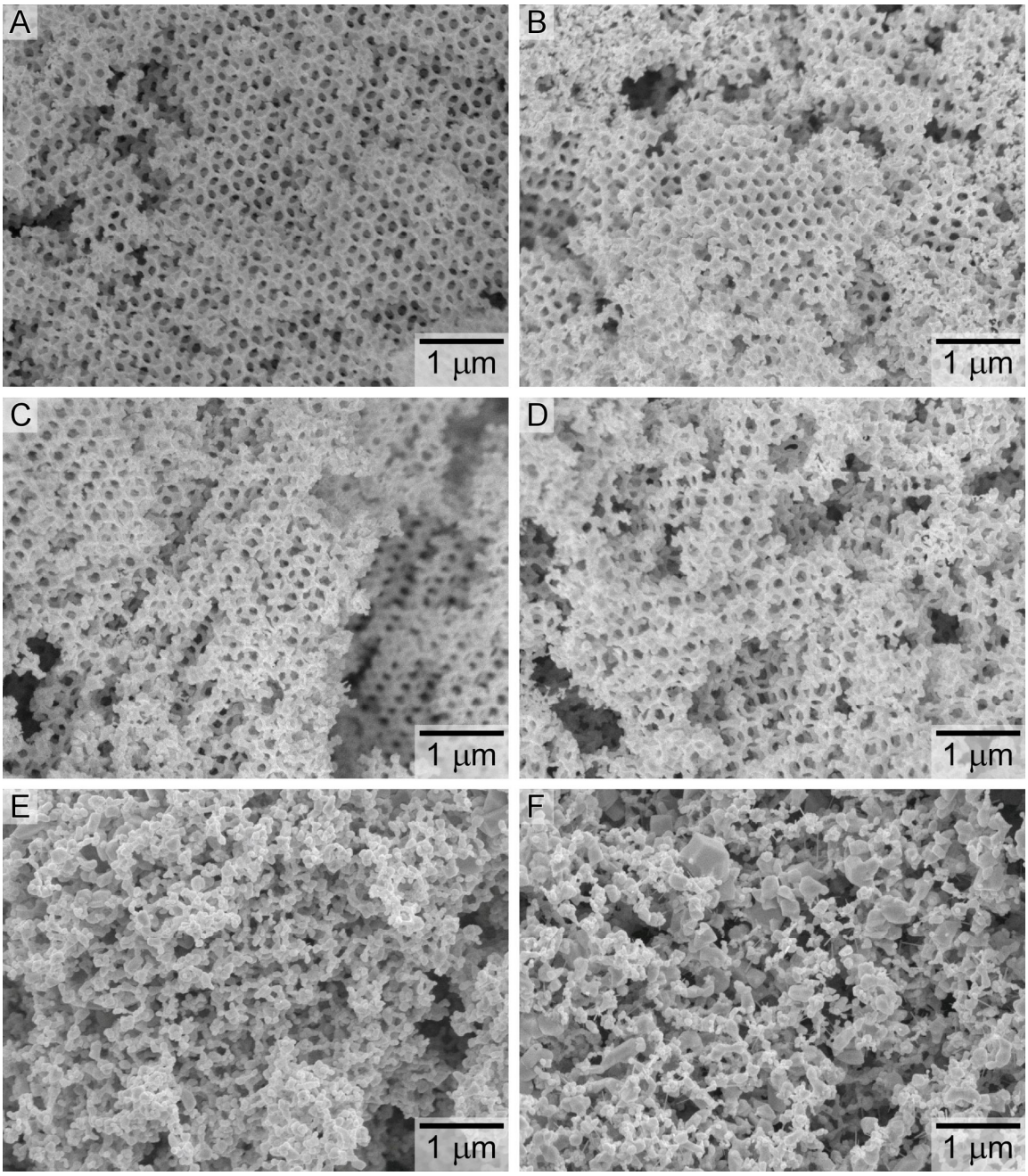

Figure 4.6. SEM images of 3DOM WMo alloys produced from AMT-AMo. (A) Sample before radiative heating. (B) Product after radiative heating in nitrogen flowing at 0.5 $L \cdot min^{-1}$ at 800°C for 30 min. (C) Product heated at 800 °C for 1 h. (D) Product heated at 800 °C for 4 h. (E) Product heated at 1000 °C for 30 min. (F) Product heated at 1000 °C for 1 h. Samples A–D were originally prepared using only H_2O as the solvent, E–F using methanol/water solvent mixtures.

The 3DOM W/Mo alloy produced from APTA/APMoA also performed similarly to samples produced by AMT-AMo after thermal treatment. In Figure 4.7 A & B, SEM images revealed the structure of the new 3DOM W/Mo alloy after being heated to 800 ˚C for 30 min, showing no deformation due to heating. When the sample was heated for 2 h at 800 ˚C still no deformation was observed (Figure 4.7 C & D). However, when heated to 1000 ˚C for 30 min, the sample exhibited significant grain growth (Figure 4.8). For the 1000 ˚C sample, the layered structure formed by the CC was still barely noticeable though the coarsening roughened the surface and distorted the windows to the point that photonic crystal properties relying on a periodic structure would be lost. To ensure that the coarsening was not caused by the loss of Mo, the 1000 ˚C sample was tested by ICP-mass spectrometry and was found to contain 4.95 wt% Mo. The results of heating to 800 and 1000 ˚C correlated well to the previous results for the 3DOM W/Mo alloy using the AMT-AMo precursors.

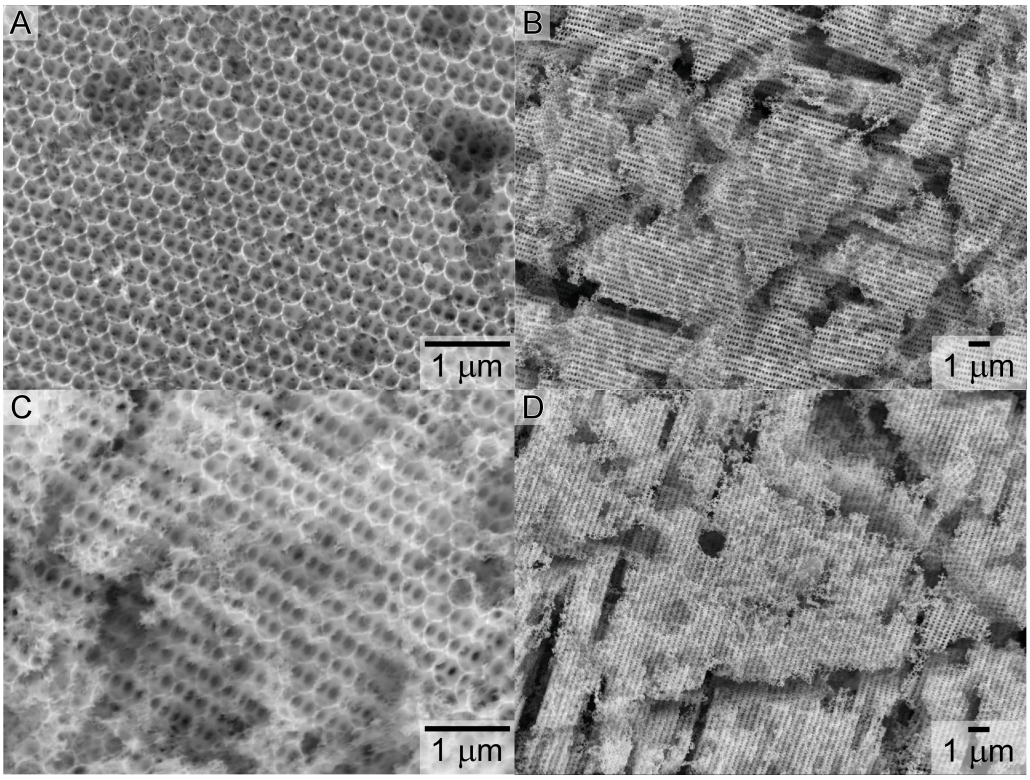

Figure 4.7. SEM images of the 3DOM W/Mo alloy (95/5 wt%) produced from APTA/APMoA. (A & B) show images of the 3DOM W/Mo sample after being heated for 30 min at 800 ˚C in a nitrogen atmosphere. (C & D) show images of the 3DOM W/Mo sample after being heated for 2 h at 800 ˚C in a nitrogen atmosphere.

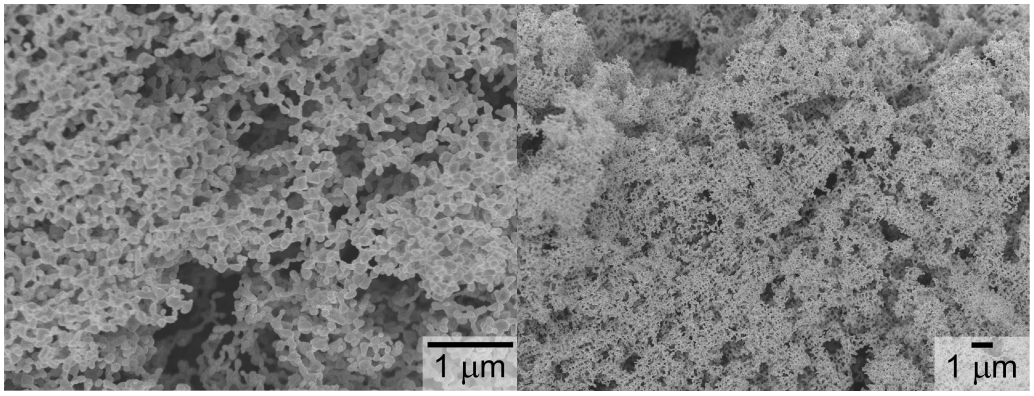

Figure 4.8. SEM images of the 3DOM W/Mo alloy (95/5 wt%) produced from APTA/APMoA after being heated for 30 min at 1000 ˚C in a nitrogen atmosphere.

4.4. Conclusion

As free-standing monolithic structures, these 3DOM W samples can be resistively heated to evaluate thermal emission without the need of an underlying support. Because of their small structural dimensions and relatively large interfacial areas, the heated materials readily react with trace amounts of water, leading to tungsten needle formation by chemical vapor transport, which is believed to involve the well-known volatile $WO_2(OH)_2$ phase. In addition, grain growth occurring during Joule heating or radiative heating of the 3DOM W samples at temperatures as low as 800 °C can destroy the periodic structure of the photonic crystal, which would lead to deterioration of its photonic properties. It should be noted that in these investigations, PMMA spheres with diameters of 540 nm were used as templates mainly for synthetic convenience. Metallic photonic crystals designed to modify emission in the infrared region of the spectrum would require larger macropores templated from larger spheres. The resulting structures would have slightly larger wall thicknesses, which may reduce structural changes to some degree. However, a more reliable means of maintaining structural integrity during heat treatments was found by alloying 3DOM W with ca. 3–5 wt% Mo. Alloy formation effectively suppressed needle formation during heat treatment, even when trace water was present in the surrounding atmosphere. Furthermore, it significantly decreased grain growth at 800 °C, so that the 3DOM structure could be maintained at this temperature for at least 4 h. Again, this stabilizing effect should be greater for tungsten photonic crystals with larger structural features and smaller specific surface areas. The advances described in this chapter, formation of a monolithic refractory metal alloys with a periodic

macroporous structure on an optical length scale, production of a relatively open structure, and thermal stabilization by alloy formation, provide important new opportunities for the design of metallic photonic crystals for thermal emission control. A more detailed study to determine the effect of Mo on the thermal stability is outlined in the following chapter.

Chapter 5

An In-situ Study of Grain Coarsening in Metallic Photonic Crystals

Outline

The following TEM characterization was performed by Fan Li.

5.1. Introduction

Previously the syntheses of 3-dimensionally ordered macroporous (3DOM) tungsten and tungsten molybdenum alloy monoliths were discussed.[92,93] Producing the 3DOM monoliths by solution methods[92] allowed us to form more open photonic crystal structures than are achievable by alternate methods, such as CVD infiltration of a colloidal crystal.[15] Such open structures are required to mitigate light absorption by the metallic skeleton.[16] We also reported thermally induced coarsening of the 3DOM tungsten skeleton and the retardation of that coarsening by the incorporation of molybdenum as an alloy at 5 wt%.[93] The effects of grain coarsening on tungsten carbide materials alloyed or doped with cobalt has been long studied and determined to be dominated by creep.[103-108] The materials however have much larger grain sizes on the order of μm which do not always exhibit coarsening on the same scale.[109] Larger grained non-sag tungsten has also been extensively studied for grain coarsening at higher temperatures upwards of 1600+ ˚C but again involves larger grains.[100,110] In addition, grain coarsening of larger tungsten grains has been studied, identifying the diffusion at dislocations as the primary mechanism for coarsening at temperatures below 2100 ˚C.[23,111-113] However, the grain growth of nanosized grains of tungsten has not been extensively investigated and the effect of molybdenum alloys in the structure is not known.[109] Nanoparticles of WS_2 were investigated by in situ TEM heating and the particles grew into hollow onion like structures at elevated temperatures.[114] In this

chapter the effects of grain coarsening will be studied by in-situ TEM measurements of both 3DOM W and 3DOM W/Mo alloys to shed light on how the molybdenum decreases the amount of grain coarsening in these samples.

5.2. Experimental

5.2.1. Materials

3DOM W was prepared as outlined in Chapter 3 for APTA2 precursor. 3DOM W/Mo was prepared as outlined in Chapter 4 for the APTA/APMoA precursor.

5.2.2. TEM preparation

Samples of 3DOM W and 3DOM W/Mo alloy(95/5 wt%) were sonicated in ethanol and dripped onto lacey carbon-film-coated Mo grids.

5.2.3. TEM in-situ heating

A FEI Tecnai T12 TEM was employed using a 120 kV accelerating voltage. In the TEM the heating stage was heated to 1000 ˚C with a dwell of 30 min and ramp rate of approximately 25 ˚C·min^{-1}.

5.3. Results and discussion

5.3.1. In-situ heating of 3DOM W

To have a better understanding of the mechanism of grain coarsening, 3DOM W was heated in-situ in a TEM under dynamic vacuum. This allowed for real time recording of

the material changes at high magnification during the entire time the sample was heated. It is important to note here that Mo grids were employed for this experiment as, at higher temperatures (800 ˚C), the typically-used copper grids would deposit copper across the entire sample and form clusters on the 3DOM metal samples and across the entire lacey carbon film. The TEM images of the as-synthesized 3DOM W sample (Figure 5.1 A & C) revealed the surface texture of the 3DOM W skeleton produced from the APTA2 precursor discussed previously in Chapter 3. As the sample was heated to 1000 ˚C, coarsening was seen and could be followed in the TEM images. In Figure 5.1 B & D, the TEM images reveal a smoother surface structure in the sample after dwelling at 1000 ˚C for 30 min, but the structure was also comprised of visibly fewer grains, though these grains had not grown so large that the 3DOM structure was lost. The boxes in Figure 5.1 A & B reveal the grain coarsening where smaller grains can be seen in image A and fewer larger grains can be seen in image B. Grain coarsening can be further observed in Figure 5.2 where TEM images at 700 (A), 900 (B) and 1000 ˚C (C-I at different dwell times) can be seen. In the TEM images here, it was revealed that the grain growth reduced the number of grains, in particular the loss of the grain highlighted by the arrow in images A & C could be tracked through the image array (Figure 5.2). In Figure 5.2, in the area highlighted by the box in image A, it can be seen that the nodule structure was completely coarsened over the same time period. From the SEM images in Figure 5.1 C & D, the wall thicknesses at the middle of the strut narrowed slightly from an average of 53±7 nm to 47±9 nm. In fact the grain coarsening to this point smoothed the structure and the coarsening may actually improve the photonic properties of this sample. However,

given enough time, it is not known if the sample coarsens to such a degree that the photonic properties diminish and are eventually lost.

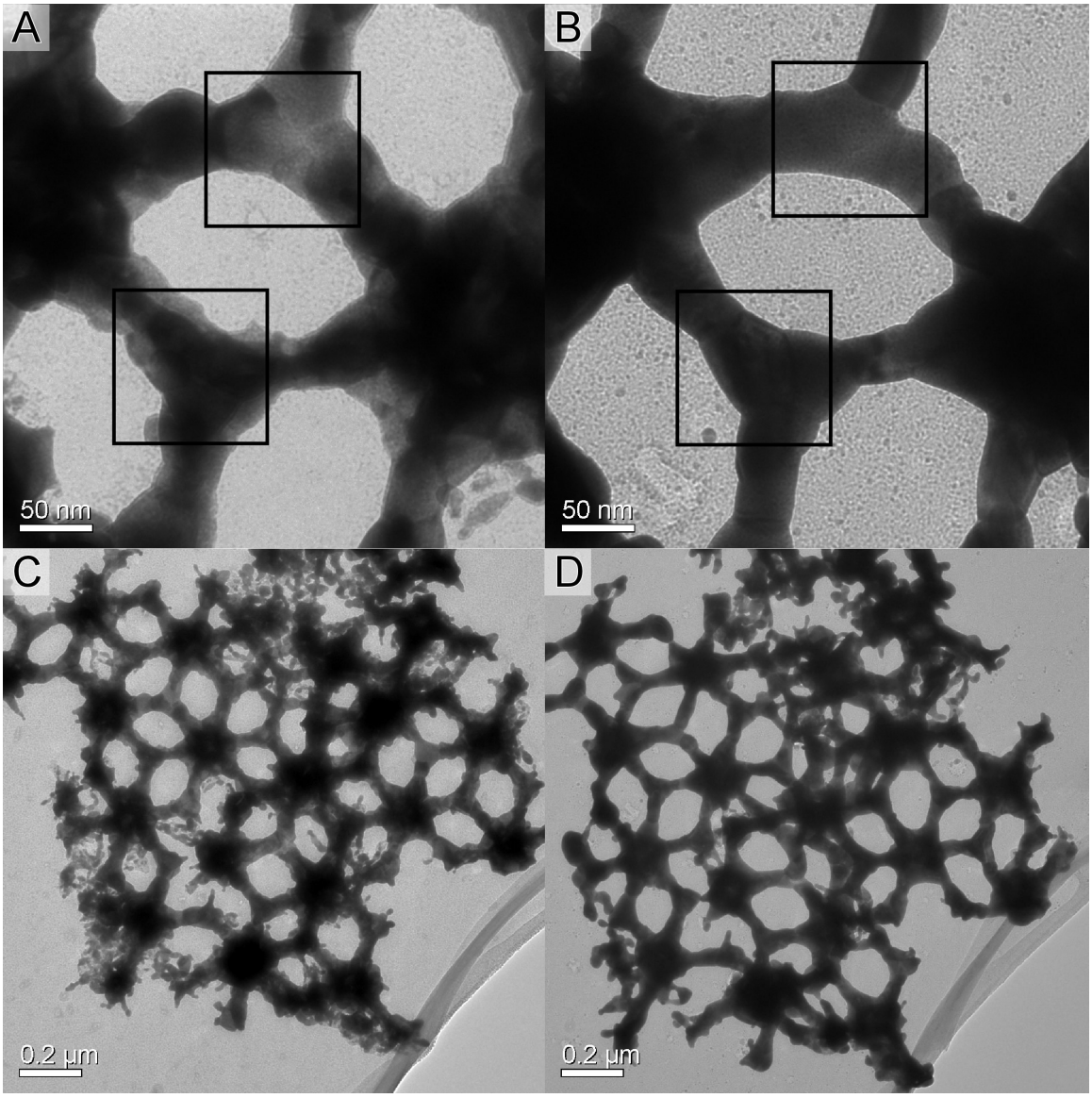

Figure 5.1. TEM images of 3DOM W from APTA at 25 ˚C (A & C) and after (B & D) in-situ heating to 1000 ˚C with a dwell time of 30 min.

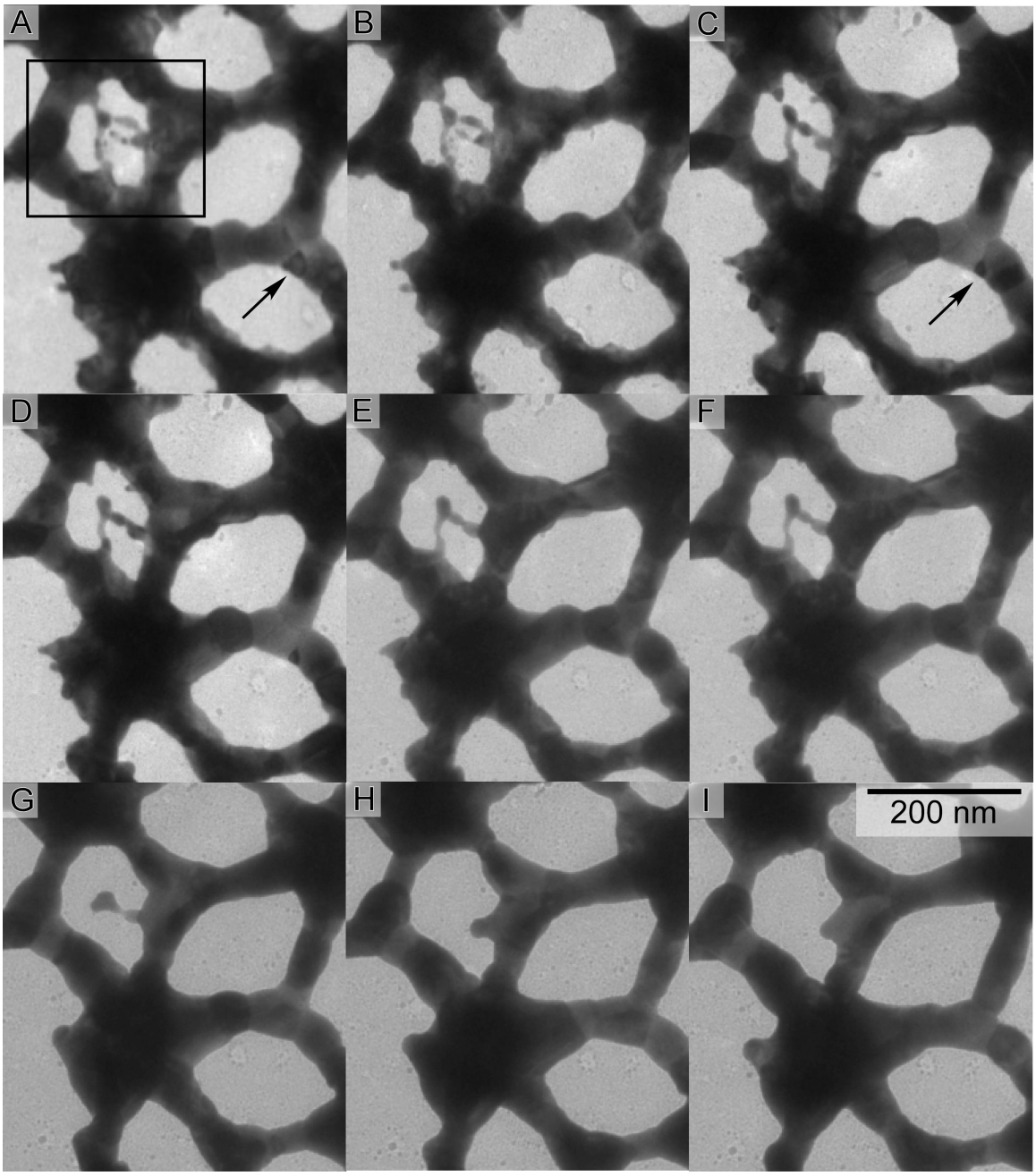

Figure 5.2. TEM images of 3DOM W during various stages of in-situ heating. (a) image at 700 ºC. (b) image at 900 ºC. (c-i) images at 1000 ºC at a dwell time of 0, 5, 10, 15, 20, 25 and 30 min.

Heating the 3DOM W sample in the TEM did not correlate directly with previous results when samples were heated as described in Chapter 5. Previous experiments indicated that by heating 3DOM W in vacuum (1×10^{-4} torr), all water can be removed from the system, which prevented the highly volatile phase of tungsten oxide from being produced and inhibited the formation of tungsten needle structures (needles were seen in samples heated in an atmosphere that contained even trace amounts of water), but large amounts of grain coarsening were observed when the sample was heated in a nitrogen atmosphere. During in-situ heating in the TEM the sample was in a high vacuum environment (1×10^{-7} torr) which removed all water from the system and eliminated any effects that gases (N_2, O_2) may have had. One possible problem in the TEM analysis may have been limited heat transfer to the sample, if it was not in direct contact with the supporting grid. The samples imaged were in direct contact with the grid and after heating exhibited coarsening similar to that of the previous sample (Figure 5.3). The areas imaged in Figure 5.3 were also 100 μm away from the area directly under the beam during the 30 minute dwell period at 1000 ˚C to eliminate any possible effects from the beam. The stage employed for in-situ heating had a maximum operating temperature of 1000 ˚C and a limited dwell time of 30 min.

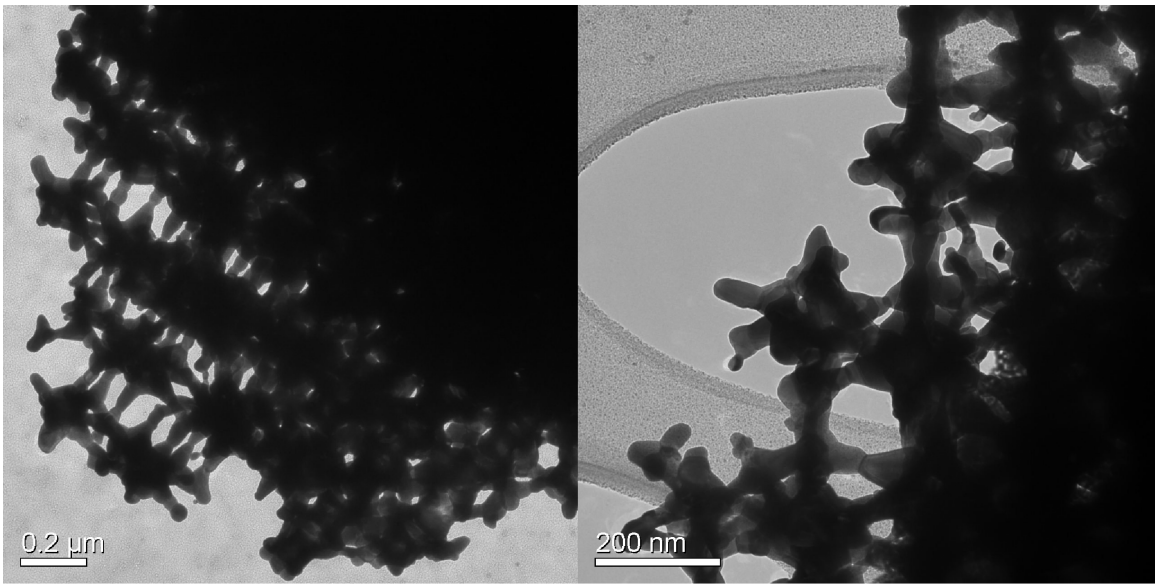

Figure 5.3. TEM images of 3DOM W after in-situ heating to 1000 ˚C. The 3DOM W pieces were in direct contact with the grid and exhibit coarsening.

5.3.2. In-situ heating of 3DOM W/Mo alloy

For the in-situ heating of 3DOM W/Mo, a sample overlapping with the grid was chosen. The TEM images shown in Figure 5.4 A & C reveal the initial structure, which contained a number of small protrusions from the skeleton and wispy tendrils attached to those protrusions, similar to the previous 3DOM W sample. After heating at 1000 ˚C for 30 min, the appearance of the sample had not changed significantly (Figure 5.4 B & D). In Figure 5.4, it was easiest to see the changes in the grain structure of the sample in the higher magnification images A & B, which revealed little change in the grain size due to coarsening. Only the thin tips of the smaller wispy tendrils were removed by coarsening processes, whereas there was little change to the larger grains. This was a good indication that the Mo in the alloy plays a role in reducing grain growth in addition to eliminating the volatile tungsten oxide and needle formation.

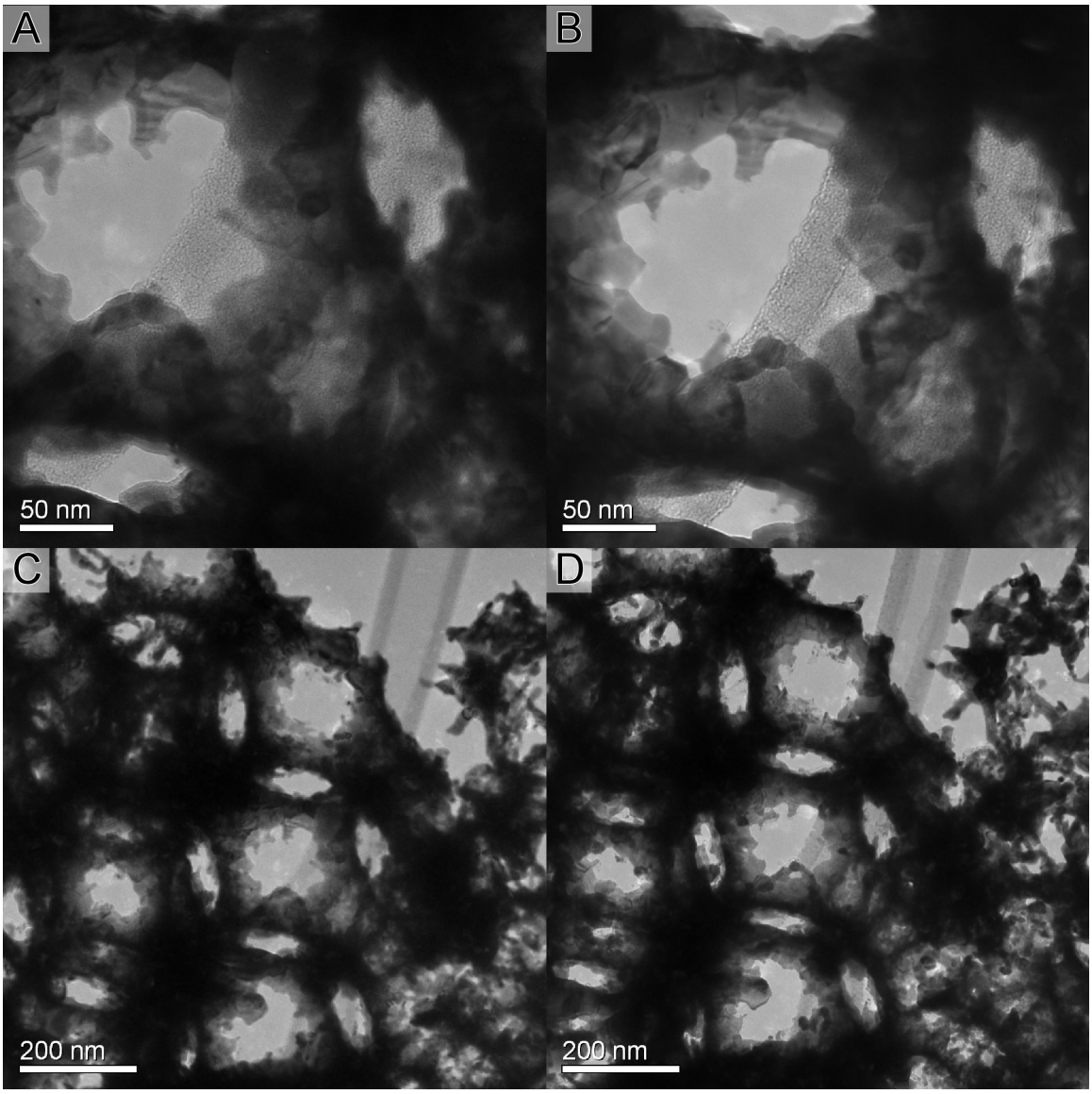

Figure 5.4. TEM images of 3DOM W/Mo alloy (95/5 wt%) at 25 ˚C (A & C) and after (B & D) heating to 1000 ˚C for 30 min.

Again areas that were away from the beam during heating were imaged to determine the extent of coarsening throughout the sample. The TEM image in Figure 5.5 A revealed a piece of 3DOM W/Mo that was in direct contact with the Mo grid and exhibited

coarsening to a similar degree to that of the area that was under the beam for the 30 minute dwell. The image in Figure 5.5 B reveals a piece of 3DOM W/Mo that was not in contact with the Mo grid. Areas of the piece of 3DOM W/Mo that were not supported directly by the lacey carbon appear to have a similar structure as those in contact with the lacey carbon. However, as there appeared to be little to no coarsening, it is impossible to determine it the thermal conductivity of the lacey carbon differed to that of the grid at 1000 ˚C. Those areas in contact with the Mo grid or just the lacey carbon did not appear to contain areas that were significantly coarsened.

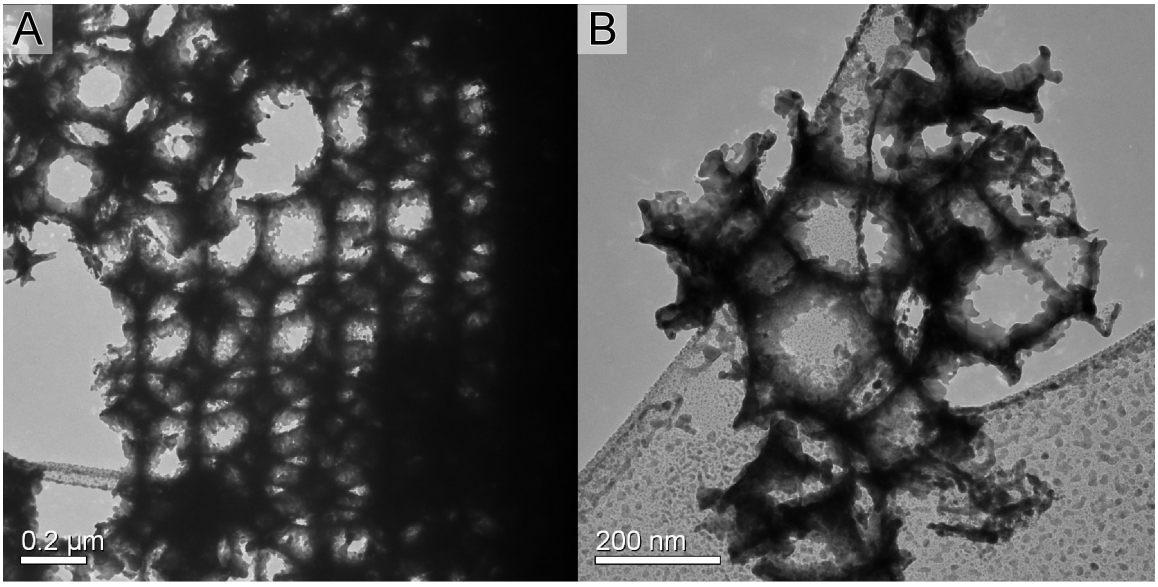

Figure 5.5. TEM images of areas away from the beam for the 3DOM W/Mo alloy after heating at 1000 ˚C for 30 min. Image A shows a piece of 3DOM W/Mo that overlaps with the grid. Image B shows a piece of 3DOM W/Mo that does not overlap with the grid.

5.4. Conclusion

The grain coarsening of these samples was dominated by grain boundary diffusion[115] but other effects mitigated the diffusion in the Mo containing sample. The coarsening effects in the previous samples were highly dependant on temperature and atmosphere which accelerated diffusion of the surface atoms.[114] For a 3DOM W sample the coarsening quickened considerably at 1000 ˚C compared to 800 ˚C when an atmosphere of nitrogen was present.[93] On the other hand, when the atmosphere was removed and the sample was heated to 1000 ˚C for 30 minutes, considerably less grain growth occurred. However, from the TEM images it was evident that areas where a few smaller grains were originally present were now comprised of single grains.

For the 3DOM W/Mo samples produced from APTA/APMoA there were very similar results to the W case when comparing atmosphere to vacuum and temperature changes. However in the W/Mo case, a lesser amount of grain coarsening was observed. Here the Mo was most likely pinning the dislocations to prevent diffusion similar to the potassium bubbles in non-sag tungsten.[100] This is also a very similar result to other additions to structures that decrease the diffusion of dislocations in the structure, including nanoparticles[116] and mesoporous structures[117].

Chapter 6

In Review and Over the Horizon

Outline

6.1 In review

6.2 Over the horizon

6.1. In review

In this work, the fabrication of monolithic 3DOM metallic photonic crystals was achieved. To reach this goal, a number of variables were optimized to create 3DOM W and 3DOM Mo materials. These variables include precursor type, solution and concentration and reduction conditions. Reduction conditions were optimized using the WCl_6 precursor system and were determined to be a maximum temperature of 800 ºC, 1 h dwell, ramp rate of 5 ºC·min^{-1}, and a H_2 containing atmosphere flowing at 0.5 L·min^{-1}.

A number of different precursors and solutions were used in this work. For W materials the precursors WCl_6, $W(EtO)_5$, tungstic acid, peroxotungstic acid, ammonium metatungstate (AMT) and an acetylated peroxotungstic acid (APTA) were employed. Tungstic acid and peroxotungstic acid were not sufficiently soluble in the solvents necessary for infiltration into the poly(methyl methacrylate) (PMMA) colloidal crystal. The WCl_6 and $W(EtO)_5$ systems only produced 3DOM granules. APTA produced a monolithic sample 3DOM W after changing to a H_2O:methanol mixed solvent, increasing the precursor concentration and changing the reducing atmosphere to pure H_2. AMT also produced a monolithic sample of 3DOM W. 3DOM W samples prepared from APTA and AMT possessed the highly open structures required for photonic crystals[16].

For 3DOM Mo both ammonium molybdate (AMo) and an acetylated peroxomolybdic acid (APMoA) were studied as precursors. Both precursors, after solvent optimization, produced partial monolithic samples. Mo was hypothesized to render highly conjugated

and aggregated polyoxometalates[98,99] which hindered infiltration and contributed to the formation of the partial monolithic samples.

Additionally, monolithic 3DOM alloys of W and Mo were prepared. Samples comprising of 95:5 or 97:3 wt% of W:Mo were synthesized from precursor combinations of APTA and APTMoA or AMT and AMo respectively. These precursors produced well ordered 3DOM W/Mo monoliths.

Joule heating of monolithic 3DOM W resulted in grain coarsening and needle formation. Needle formation was caused by a highly volatile $WO_2(OH)_2$ phase.[23] The needle formation could be eliminated with rigorous removal of H_2O from the testing device but grain coarsening remained a difficulty. 3DOM W/Mo alloys also reduced and could even eliminate needle formation at temperatures up to and at 800 ºC.

Grain coarsening was studied by radiative heating in flowing N_2. 3DOM W exhibited coarsening at 800 ºC. By alloying W with Mo (95:5 wt% W:Mo), the 3DOM W/Mo sample did not coarsen at 800 ºC but did coarsen at 1000 ºC. This was an interesting result and was studied further with TEM and in-situ heating.

3DOM W and 3DOM W/Mo samples were heated to 1000 ºC in a TEM and held at 1000 ºC for 30 min to study grain coarsening in real time. The 3DOM W sample coarsened slightly at 1000 ºC whereas the 3DOM Mo sample exhibited almost no change. Grain

coarsening in the 3DOM samples is dominated by grain boundary diffusion through dislocations.[115] The reduction of coarsening in both samples could be attributed to the high vacuum (1×10^{-7} torr), without a gas atmosphere there was no surface diffusion which limited grain coarsening.[114,118] The 3DOM W/Mo sample exhibited no coarsening, this was attributed to the Mo pinning dislocations, which then caused a decrease in grain coarsening.[100] Further study is needed at higher temperatures to observe changes in the grain structure that will occur when the material is used as a filament.

In this thesis work great strides have been made in the fabrication of 3DOM metallic photonic crystals towards thermal emission. An easy to replicate, benchtop synthetic technique was developed to produce 3DOM W, Mo, W/Mo alloys and W_2C using the new precursors APTA and APMoA. The 3DOM materials comprised of W, W_xC and W/Mo alloy (95:5 wt%) where produced in monolithic form which is 1000s of layers thick, compared to 10s of layers thick for typical thin film and lithographic techniques. Materials on the monolithic scale have not been produced by any other method than solution infiltration. Even then, this is only the third example of a nanoporous monolithic self supporting material.[21,22] The ability to generate monolithic 3DOM materials (after reduction) with highly open pore structures allowed us to confirm theoretical results that photonic effects are possible in metallic photonic crystals prepared by colloidal crystal templating techniques.[16] The introduction of Mo as an alloy into 3DOM W not only eliminated the volatile phase, but it also increased the working temperature in an inert atmosphere up to temperatures similar to those studied previously only in vacuum.[12] The

effect Mo has on pinning dislocations in 3DOM W was also determined in this work by a TEM in situ heating study.

6.2. Over the horizon

Beyond continued studies of the nanostructure at increased temperature a few materials adjustments must be made. The most relevant change needs to be an increase in the template sphere size. As of now, the 3DOM W and 3DOM W/Mo produced in this work exhibit stop bands in the visible region. Recent progress by David Josephson (University of Minnesota, Department of Chemistry) has been made to produce ~2 μm polystyrene spheres with a low polydispersity in spheres size (<5%) that can be ordered into a colloidal crystal by a micro-capillary plane (molding) technique. Producing thin films leads to another adjustment, the 40% shrinkage from template sphere size to pore size, in the 3DOM W or 3DOM W/Mo materials in this work, causes such an immense stress that the product is in a granular form and not a continuous thin film. This is caused by the interaction of the substrate with the thin film and anchoring in place the first plane of spheres that then causes shear stress as the regions above shrink in size by 40%. To produce 3DOM W and 3DOM W/Mo in thin film form using solution techniques described in this work will be a daunting task. Some of the stress could be mitigated by employing a polymer membrane over the structure to reduce cracking in the thin film.[119]

Alternatively, the infiltration method could be changed to CVD or ALD but then the window sizes would be too small for the material to exhibit photonic effects. Here too

this can be overcome by annealing the spheres together near the glass transition temperature (105 ºC). The reduced size of the infiltration pores should not make employing CVD or ALD difficult, the difficult part will come in determining the optimal temperature and time to anneal the spheres so a sufficiently open structure can be formed. The art of annealing the template could be used to open up the structure of any inverse structure, including opening up the structure of solution based precursors that exhibit surface templating characteristics.

However the future might be to produce 3DOM W materials through electrodeposition. The electrodeposition of W has been reported to take place in molten salts at 250 ºC .[120] While this will technique will not be useful for polymer colloidal crystals, it can be used for silica colloidal crystals.

Another promising method would be to apply thin coatings of the metals on the surface of another material that can withstand the higher temperatures; one such material is carbon and can be easily made in a 3DOM monolithic form[22]. Applying a W film to a 3DOM C monolith through ALD has already been achieved by Dr. Shaibal K. Sarkar (University of Colorado at Boulder, Department of Chemistry and Biochemistry) (Figure 6.1 a) and through CVD by Prashant Nagpal (University of Minnesota, Department of Chemical Engineering). Now the system needs to be optimized in the same manner as the 3DOM W system above. Furthermore, large openings can be created by oxygen plasma etching the 3DOM C prior to applying the W coating. Initial radiative heating tests

indicate that the W coated 3DOM C samples will coarsen at 1000 ºC (Figure 6.1 b). The reduced amount of coarsening is believed to be attributed to the ALD technique producing films with fewer defects. 3DOM C composites with a surface coating of W/Mo alloy have not been obtained yet.

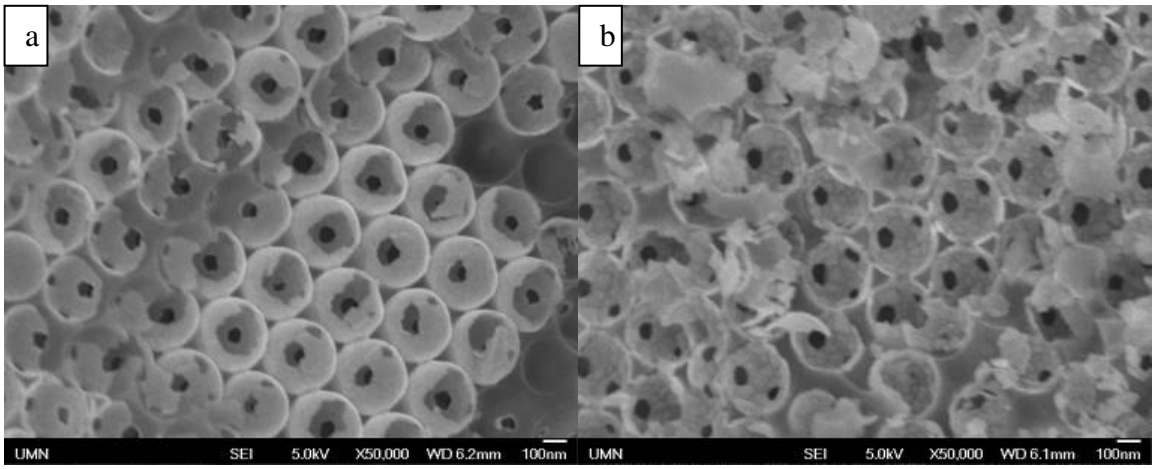

Figure 6.1. SEM images of 3DOM C coated with 10 nm of W by ALD.[5] (a) SEM image of 3DOM C coated W after conversion to the α-phase by reduction in H_2 with a 1 h dwell time. (b) SEM image of sample (a) after radiative heating in N_2 with a 1 h dwell time.

Though, even with the 3DOM W/Mo sample, there may still be too much grain coarsening in the samples at the elevated temperatures required for lighting, there are other possible applications for these materials. Recently a W woodpile photonic crystal structure was studied for use in a thermophotovoltaic device.[91] The W woodpile structure would act as a thermal collector and narrow band emitter to increase the efficiency of a solar cell by up to 30%.

[5] 3DOM C synthesized by Nicholas Denny and coated using ALD by Dr. Shaibal K. Sarkar, University of Colorado at Boulder, Steven George Group.

Another application may come in the form of thermal camouflage. If a vehicle is covered in paint that incorporates 3DOM materials that have stop bands in the infrared, it is possible to reflect the heat generated by the vehicle into the ground. If the heat can be channeled away from the vehicle then the vehicle would not be able to be targeted by heat seeking missiles or be as visible at night when viewed by thermal night vision goggles. It is a little poetic that the next generation of kinetic projectiles are comprised of tungsten (to replace depleted uranium)[121] and tungsten could make it harder to see the target.

In conclusion, 3DOM metallic photonic crystals may never be able to retain their nanostructure at high enough temperatures to compete with fluorescent or LED lamps for lighting efficiency. However, 3DOM metallic photonic crystals could have a bright future in possibly saving our ice caps by producing green energy through thermophotovoltaics.

Chapter 7

References

(1) Eckelman, M. J.; Anastas, P. T.; Zimmerman, J. B. *Environ. Sci. Technol.* **2008**, *42*, 8564-8570.
(2) MacIsaac, D.; Kanner, G.; Anderson, G. *The Physics Teacher* **1999**, *37*, 520-525.
(3) John, S. *Phys. Rev. Lett.* **1987**, *58*, 2486-2489.
(4) Yablonovitch, E. *Phys. Rev. Lett.* **1987**, *58*, 2059-2062.
(5) Lopez, C. *Adv. Mater.* **2003**, *15*, 1679-1705.
(6) Schroden, R. C.; Al-Daous, M.; Blanford, C. F.; Stein, A. *Chem. Mater.* **2002**, *14*, 3305-3315.
(7) Busch, K.; John, S. *Phys. Rev. E: Stat., Nonlinear, Soft Matter Phys.* **1998**, *58*, 3896-3908.
(8) Fleming, J. G.; Lin, S. Y.; El-Kady, I.; Biswas, R.; Ho, K. M. *Nature* **2002**, *417*, 52-55.
(9) Lin, S. Y.; Fleming, J. G.; El-Kady, I. *Opt. Lett.* **2003**, *28*, 1683-1685.
(10) Lin, S. Y.; Fleming, J. G.; El-Kady, I. *Appl. Phys. Lett.* **2003**, *83*, 593-595.
(11) Lin, S. Y.; Fleming, J. G.; Li, Z. Y.; El-Kady, I.; Biswas, R.; Ho, K. M. *J. Opt. Soc. Am. B* **2003**, *20*, 1538-1541.
(12) Lin, S. Y.; Moreno, J.; Fleming, J. G. *Appl. Phys. Lett.* **2003**, *83*, 380-382.
(13) Lin, S.-Y.; Fleming, J. G.; El-Kady, I. *Opt. Lett.* **2003**, *28*, 1909-1911.
(14) Walsh, T. A.; Bur, J. A.; Kim, Y.-S.; Lu, T.-M.; Lin, S.-Y. *J. Opt. Soc. Am. B* **2009**, *26*, 1450-1455.
(15) Von Freymann, G.; John, S.; Schulz-Dobrick, M.; Vekris, E.; Tetreault, N.; Wong, S.; Kitaev, V.; Ozin, G. A. *Appl. Phys. Lett.* **2004**, *84*, 224-226.
(16) Han, S. E.; Stein, A.; Norris, D. J. *Phys. Rev. Lett.* **2007**, *99*, 053906/1-053906/4.
(17) Blanford, C. F.; Carter, C. B.; Stein, A. *J. Phys.: Conf. Ser.* **2005**, *26*, 264-267.
(18) *CRC Handbook of Chemistry and Physics*; 83 ed.; Lide, D. R., Ed.; CRC Press LLC: Boca Raton, 2002-2003; Vol. 83.
(19) Lytle, J. C.; Stein, A. *Annu. Rev. Nano Res.* **2006**, *1*, 1-79.
(20) Stein, A.; Li, F.; Denny, N. R. *Chem. Mater.* **2008**, *20*, 649-666.
(21) Wang, Z.; Li, F.; Ergang, N. S.; Stein, A. *Chem. Mater.* **2006**, *18*, 5543-5553.
(22) Lee, K. T.; Lytle, J. C.; Ergang, N. S.; Oh, S. M.; Stein, A. *Adv. Funct. Mater.* **2005**, *15*, 547-556.
(23) Lassner, E.; Schubert, W.-D. *Tungsten: Properties, Chemistry, Technology of the Element, Alloys, and Chemical Compounds*; Kluwer Academic / Plenum Publishers: New York, 1999.
(24) McKelvy, M. J.; Mitan, P.; Hintze, K.; Patrick, E.; Allagadda, K.; Ramakrishna, B. L.; Denny, C.; Pryor, B.; Chizmeshya, A. V. G.; Pizziconi, V. *Mater. Res. Soc. Symp. Proc.* **2000**, *632E*, HH7.2.1-HH7.2.6.
(25) Widagdo, S. *Ind. Eng. Chem. Res.* **2006**, *45*, 8231-8233.
(26) Hiramoto, H.; Sakamoto, H.; (Stanley Electric Co., Ltd., Japan). JP Patent 98-316303 2000149879, 2000.

(27) Kawakatsu, A.; (Toshiba Lighting & Technology, Japan). JP Patent 95-72005 08273630, 1996.
(28) Wei, J.; Zhu, H.; Wu, D.; Wei, B. *Appl. Phys. Lett.* **2004**, *84*, 4869-4871.
(29) Fischer, A. *Photonics Spectra* **2009**, *43*, 106.
(30) Gu, Z.-Z.; Uetsuka, H.; Takahashi, K.; Nakajima, R.; Onishi, H.; Fujishima, A.; Sato, O. *Angew. Chem., Int. Ed.* **2003**, *42*, 894-897.
(31) Kustandi, T. S.; Low, H. Y.; Teng, J. H.; Rodriguez, I.; Yin, R. *Small* **2009**, *5*, 574-578.
(32) Jones, J. B.; Sanders, J. V.; Segnit, E. R. *Nature* **1964**, *204*, 990-991.
(33) Kavtreva, O. A.; Ankudinov, A. V.; Bazhenova, A. G.; Kumzerov, Y. A.; Limonov, M. F.; Samusev, K. B.; Sel'kin, A. V. *Phys. Solid State* **2007**, *49*, 708-714.
(34) Mandal, S.; Erickson, D. *Opt. Express* **2008**, *16*, 1623-31.
(35) Chen, Q.; Allsopp, D. W. E. *Opt. Commun.* **2008**, *281*, 5771-5774.
(36) Gerard, J. M.; Izrael, A.; Marzin, J. Y.; Padjen, R.; Ladan, F. R. *Solid-State Electron.* **1994**, *37*, 1341-1344.
(37) Do, Y. R.; Kim, Y.-C.; Song, Y.-W.; Lee, Y.-H. *J. Appl. Phys.* **2004**, *96*, 7629-7636.
(38) Chang, Y.-C.; Wu, H.-W.; Chen, H.-L.; Wang, W.-Y.; Chen, L.-J. *J. Phys. Chem.*, ACS ASAP.
(39) Wang, B.; Zhao, W.; Chen, A.; Chua, S.-J. *J. Cryst. Growth* **2006**, *288*, 200-204.
(40) Nagpal, P.; Lindquist, N. C.; Oh, S.-H.; Norris, D. J. *Science* **2009**, *325*, 594-597.
(41) Mekis, A.; Chen, J. C.; Kurland, I.; Fan, S.; Villeneuve, P. R.; Joannopoulos, J. D. *Phys. Rev. Lett.* **1996**, *77*, 3787-3790.
(42) Dong, G. Y.; Yang, X. L.; Cai, L. Z.; Shen, X. X.; Wang, Y. R. *Opt. Express* **2008**, *16*, 15375-15381.
(43) Saravanamuttu, K.; Blanford, C. F.; Sharp, D. N.; Dedman, E. R.; Turberfield, A. J.; Denning, R. G. *Chem. Mater.* **2003**, *15*, 2301-2304.
(44) Yablonovitch, E.; Gmitter, T. J.; Leung, K. M. *Phys. Rev. Lett.* **1991**, *67*, 2295-8.
(45) Moon, J. H.; Small, A.; Yi, G.-R.; Lee, S.-K.; Chang, W.-S.; Pine, D. J.; Yang, S.-M. *Synth. Met.* **2005**, *148*, 99-102.
(46) Xu, Y.; Zhu, X.; Dan, Y.; Moon, J. H.; Chen, V. W.; Johnson, A. T.; Perry, J. W.; Yang, S. *Chem. Mater.* **2008**, *20*, 1816-1823.
(47) Zhong, Y.; Wu, L.; Su, H.; Wong Kam, S.; Wang, H. *Opt. Express* **2006**, *14*, 6837-6843.
(48) Jun, Y.; Nagpal, P.; Norris, D. J. *Adv. Mater.* **2008**, *20*, 606-610.
(49) Braun, P. V.; Rinne, S. A.; Garcia-Santamaria, F. *Adv. Mater.* **2006**, *18*, 2665-2678.
(50) McCracken, J. R.; Datyner, A. *J. Appl. Polym. Sci.* **1974**, *18*, 3365-3372.
(51) Stober, W.; Fink, A.; Bohn, E. *J. Colloid Interface Sci.* **1968**, *26*, 62-69.
(52) Schroden, R. C.; Balakrishnan, N.; Stein, A. *"Inverse Opal Photonic Crystals-A Laboratory Guide," Univeristy of Minnesota Materials Research Science and Engineering Center* **2001**.
(53) Xia, Y.; Gates, B.; Li, Z.-Y. *Adv. Mater.* **2001**, *13*, 409-413.
(54) Popczun, E. J.; Josephson, D.; Stein, A. *Unpublished research* **2009**.
(55) Brewer, D. D.; Allen, J.; Miller, M. R.; de Santos, J. M.; Kumar, S.; Norris, D. J.; Tsapatsis, M.; Scriven, L. E. *Langmuir* **2008**, *24*, 13683-13693.

(56) Meng, L.; Wei, H.; Nagel, A.; Wiley Benjamin, J.; Scriven, L. E.; Norris David, J. *Nano Lett.* **2006**, *6*, 2249-2253.
(57) Liu, Z.; Jin, Z.; Li, W.; Qiu, J.; Zhao, J.; Liu, X. *Appl. Surf. Sci.* **2006**, *252*, 5002-5009.
(58) Park, S. H.; Qin, D.; Xia, Y. *Chem. Mater.* **1998**, *10*, 1745-1747.
(59) Chiappini, A.; Armellini, C.; Chiasera, A.; Ferrari, M.; Fortes, L.; Clara Goncalves, M.; Guider, R.; Jestin, Y.; Retoux, R.; Nunzi Conti, G.; Pelli, S.; Almeida, R. M.; Righini, G. C. *J. Non-Cryst. Solids* **2009**, *355*, 1167-1170.
(60) Cabanas, A.; Enciso, E.; Carbajo, M. C.; Torralvo, M. J.; Pando, C.; Renuncio, J. A. R. *Chem. Commun.* **2005**, 2618-2620.
(61) Li, F.; Wang, Z.; Ergang, N. S.; Fyfe, C. A.; Stein, A. *Langmuir* **2007**, *23*, 3996-4004.
(62) Wang, Z.; Al-Daous, M. A.; Kiesel, E. R.; Li, F.; Stein, A. *Microporous Mesoporous Mater.* **2009**, *120*, 351-358.
(63) Juarez, B. H.; Garcia, P. D.; Golmayo, D.; Blanco, A.; Lopez, C. *Adv. Mater.* **2005**, *17*, 2761-2765.
(64) Miguez, H.; Chomski, E.; Garcia-Santamaria, F.; Ibisate, M.; John, S.; Lopez, C.; Meseguer, F.; Mondia, J. P.; Ozin, G. A.; Toader, O.; Van Driel, H. M. *Adv. Mater.* **2001**, *13*, 1634-1637.
(65) Rugge, A.; Becker, J. S.; Gordon, R. G.; Tolbert, S. H. *Nano Lett.* **2003**, *3*, 1293-1297.
(66) Wang, M.; Wang, X. *Sol. Energy Mater. Sol. Cells* **2008**, *92*, 357-362.
(67) Yu, X.; Lee, Y.-J.; Furstenberg, R.; White, J. O.; Braun, P. V. *Adv. Mater.* **2007**, *19*, 1689-1692.
(68) Chen, D.; Liu, J.; Wang, P.; Zhang, L.; Ren, J.; Tang, F.; Wu, W. *Colloids Surf., A* **2007**, *302*, 461-466.
(69) Zhang, L.; D'Acunzi, M.; Kappl, M.; Auernhammer, G. K.; Vollmer, D.; van Kats, C. M.; van Blaaderen, A. *Langmuir* **2009**, *25*, 2711-2717.
(70) Eradat, N.; Huang, J. D.; Vardeny, Z. V.; Zakhidov, A. A.; Khayrullin, I.; Udod, I.; Baughman, R. H. *Synth. Met.* **2001**, *116*, 501-504.
(71) Yan, H.; Blanford, C. F.; Lytle, J. C.; Carter, C. B.; Smyrl, W. H.; Stein, A. *Chem. Mater.* **2001**, *13*, 4314-4321.
(72) Wang, D.; Salgueirino-Maceira, V.; Liz-Marzan, L. M.; Caruso, F. *Adv. Mater.* **2002**, *14*, 908-912.
(73) Tan, Y.; Qian, W.; Ding, S.; Wang, Y. *Chem. Mater.* **2006**, *18*, 3385-3389.
(74) Kuncicky, D. M.; Prevo, B. G.; Velev, O. D. *J. Mater. Chem.* **2006**, *16*, 1207-1211.
(75) Li, W.; Sun, G.; Tang, F.; Tam, W. Y.; Li, J.; Chan, C. T.; Sheng, P. *J. Phys.: Condens. Matter* **2005**, *17*, 2177-2190.
(76) Kelf, T. A.; Sugawara, Y.; Cole, R. M.; Baumberg, J. J.; Abdelsalam, M. E.; Cintra, S.; Mahajan, S.; Russell, A. E.; Bartlett, P. N. *Phys. Rev. B: Condens. Matter Mater. Phys.* **2006**, *74*, 245415/1-245415/12.
(77) Li, F.; Xu, L.; Zhou, W. L.; He, J.; Baughman, R. H.; Zakhidov, A. A.; Wiley, J. B. *Adv. Mater.* **2002**, *14*, 1528-1531.
(78) Altube, A.; Blanco, A.; Lopez, C. *Mater. Lett.* **2008**, *62*, 2677-2680.

(79) Braun, P. V.; Wiltzius, P. *Curr. Opin. Colloid Interface Sci.* **2002**, *7*, 116-123.
(80) Jiang, P.; Cizeron, J.; Bertone, J. F.; Colvin, V. L. *J. Am. Chem. Soc.* **1999**, *121*, 7957-7958.
(81) Yan, Q.; Nukala, P.; Chiang, Y.-M.; Wong, C. C. *Thin Solid Films* **2009**, *517*, 5166-5171.
(82) Xu, L.; Zhou, W.; Kozlov, M. E.; Khayrullin, I. I.; Udod, I.; Zakhidov, A. A.; Baughman, R. H.; Wiley, J. B. *J. Am. Chem. Soc.* **2001**, *123*, 763-764.
(83) Blanford, C. F.; Schroden, R. C.; Al-Daous, M.; Stein, A. *Adv. Mater.* **2001**, *13*, 26-29.
(84) Schroden, R. C.; Al-Daous, M.; Stein, A. *Chem. Mater.* **2001**, *13*, 2945-2950.
(85) Han, S. E., University of Minnesota, 2009.
(86) Celanovic, I.; Jovanovic, N.; Kassakian, J. *Appl. Phys. Lett.* **2008**, *92*, 193101/1-193101/3.
(87) Wan, J. T. K.; Chan, C. T. *Appl. Phys. Lett.* **2006**, *89*, 041915/1-041915/3.
(88) El-Kady, I.; Chow, W. W.; Fleming, J. G. *Phys. Rev. B: Condens. Matter Mater. Phys.* **2005**, *72*, 195110/1-195110/5.
(89) Chen, X.; Zhou, F.; Wang, J.; Li, M.; Jiang, L.; Song, Y.; Li, Z.; Zhu, D. *Appl. Phys. A: Mater. Sci. Process.* **2008**, *93*, 489-493.
(90) El-Kady, I.; Farfan, G. B.; Rammohan, R.; Taha, M. M. R. *Appl. Phys. Lett.* **2008**, *93*, 153501/1-153501/3.
(91) Nagpal, P.; Han, S. E.; Stein, A.; Norris, D. J. *Nano Lett.* **2008**, *8*, 3238-3243.
(92) Denny, N. R.; Han, S.; Turgeon, R. T.; Lytle, J. C.; Norris, D. J.; Stein, A. *Proc. SPIE-Int. Soc. Opt. Eng.* **2005**, *6005*, 600505/1-600505/13.
(93) Denny, N. R.; Han, S. E.; Norris, D. J.; Stein, A. *Chem. Mater.* **2007**, *19*, 4563-4569.
(94) Sharma, N.; Deepa, M.; Varshney, P.; Agnihotry, S. A. *J. Non-Cryst. Solids* **2002**, *306*, 129-137.
(95) Cronin, J. P.; Tarico, D. J.; Agrawal, A.; Zhang, R. L. US Patent 5277986, 1994.
(96) Lassner, E.; Schubert, W. D. *Tungsten*; Kluwer Academic: New York, 1999.
(97) Fleming, J. G.; Lin, S. Y.; El-Kady, I.; Biswas, R.; Ho, K. M. *Nature* **2002**, *417*, 52-55.
(98) Müller, A.; Serain, C. *Acc. Chem. Res.* **1999**, *33*, 2-10.
(99) Baes Jr., C. F.; Mesmer, R. E. *The Hydrolysis of Cations*; John Wiley and Sons: New York, 1976.
(100) Uray, L.; Sulyok, A.; Tekula-Buxbaum, P. *High Temp. Mater. Processes (Tel Aviv, Israel)* **2005**, *24*, 289-300.
(101) *The Chemistry of Non-sag Tungsten*; Bartha, L.; Lassner, E.; Schubert, W.-D.; Lux, B., Eds.; Elsevier Science, Inc: Tarrytown, 1995.
(102) Cheetham, A. K.; Chowdhury, A. J. S. *J. Less-Common Met.* **1986**, *116*, 43-50.
(103) Hayashi, K.; Matsuoka, N. *J. Adv. Mater.* **2002**, *34*, 38-48.
(104) Huang, S. G.; Liu, R. L.; Li, L.; Van der Biest, O.; Vleugels, J. *Int. J. Refract. Met. Hard Mater.* **2008**, *26*, 389-395.
(105) Li, T.; Li, Q.; Lu, L.; Fuh, J. Y. H.; Yu, P. C. *Philos. Mag.* **2008**, *87*, 5657-5671.
(106) Sommer, M.; Schubert, W.-D.; Zobetz, E.; Warbichler, P. *Int. J. Refract. Met. Hard Mater.* **2002**, *20*, 41-50.

(107) Wang, X.; Fang, Z. Z.; Sohn, H. Y. *Int. J. Refract. Met. Hard Mater.* **2008**, *26*, 232-241.
(108) Yang, D.-Y.; Kang, S.-J. L. *Int. J. Refract. Met. Hard Mater.* **2008**, *27*, 90-94.
(109) Schuh, C. A.; Nieh, T. G. *Mat. Res. Soc. Symp. Proc.* **2003**, *740*, 11.8.1-11.8.6.
(110) Samajdar, I.; Verlinden, B.; Watte, P.; Mertens, F. *Scr. Mater.* **1999**, *40*, 1263-1268.
(111) Robinson, S. L.; Sherby, O. D. *Acta Metall.* **1969**, *17*, 109-125.
(112) Almanstotter, J.; Ruhle, M. *Int. J. Refract. Met. Hard Mater.* **1997**, *15*, 295-300.
(113) Briant, C. L.; Unsal, G.; Kasper, R. B. *Interface Sci.* **1997**, *4*, 81-97.
(114) Zink, N.; Therese, H. A.; Pansiot, J.; Yella, A.; Banhart, F.; Tremel, W. *Chem. Mater.* **2008**, *20*, 65-71.
(115) Kothari, N. C. *J. Appl. Phys.* **1967**, *38*, 2395-2396.
(116) Mavoon, H.; Jin, S. In *Appl. Phys. Lett.* **1998**, 73, 2290-2292.
(117) Teoh, L. G.; Shieh, J.; Wei, H. L.; Hon, M. H. *J. Mater. Res.* **2004**, *19*, 2687-2693.
(118) Bowden, K. F.; Singer, K. E. *Nature* **1969**, *222*, 977-979.
(119) Turner, M. E.; Trentler, T. J.; Colvin, V. L. *Adv. Mater.* **2001**, *13*, 180-183.
(120) Nakajima, H.; Nohira, T.; Hagiwara, R.; Nitta, K.; Inazama, S.; Okada, K. *Electrochimica Acta* **2007**, *53*, 24-27.
(121) Dummer, T.; Lasalvia, J. C.; Ravichandran, G.; Meyers, M. A. *Acta Mater.* **1998**, *46*, 6267-6290.
(122) Gu, S.; Akama, H.; Hagao, D.; Kobayashi, Y.; Konno, M. *Langmuir* **2004**, *20*, 7948-7951.
(123) Lee, W.-C.; Lin, C.-H.; Ruaan, R.-C.; Hsu, K.-Y. *J. Chromatogr. A* **1995**, *704*, 307-314.
(124) Kamp, U.; Kitaev, V.; Von Freymann, G.; Ozin, G. A.; Mabury, S. A. *Adv. Mater.* **2005**, *17*, 438-443.

Appendix A

PMMA Synthesis and Colloidal Crystal Formation

Outline

A.1. Sphere synthesis

- A.1.1. AMPA and KPS synthesis
  - A.1.1.1. Materials
  - A.1.1.2. Synthesis and products

A.2. Colloidal crystal formation

- A.2.1. Sedimentation
- A.2.2. Convective self assembly
- A.2.3. Capillary rods

A.1. Sphere synthesis

This section discusses the synthesis of the polymer spheres used in this work to create the colloidal crystal templates. For this work the 2-2'azobis(2-mtheyl proprion amidine) (AMPA) initiated poly(methyl methacrylate) (PMMA) spheres were used as the template for the tungsten (VI) chloride, tungsten (V) ethoxide, peroxotungstic acid, tungstic acid and acetylated peroxotungstic acid (1) precursors. All other materials used the KPS–initiated PMMA spheres as the template material. Figure A.1 is a pictorial of the PMMA sphere synthesis and colloidal crystal formation.

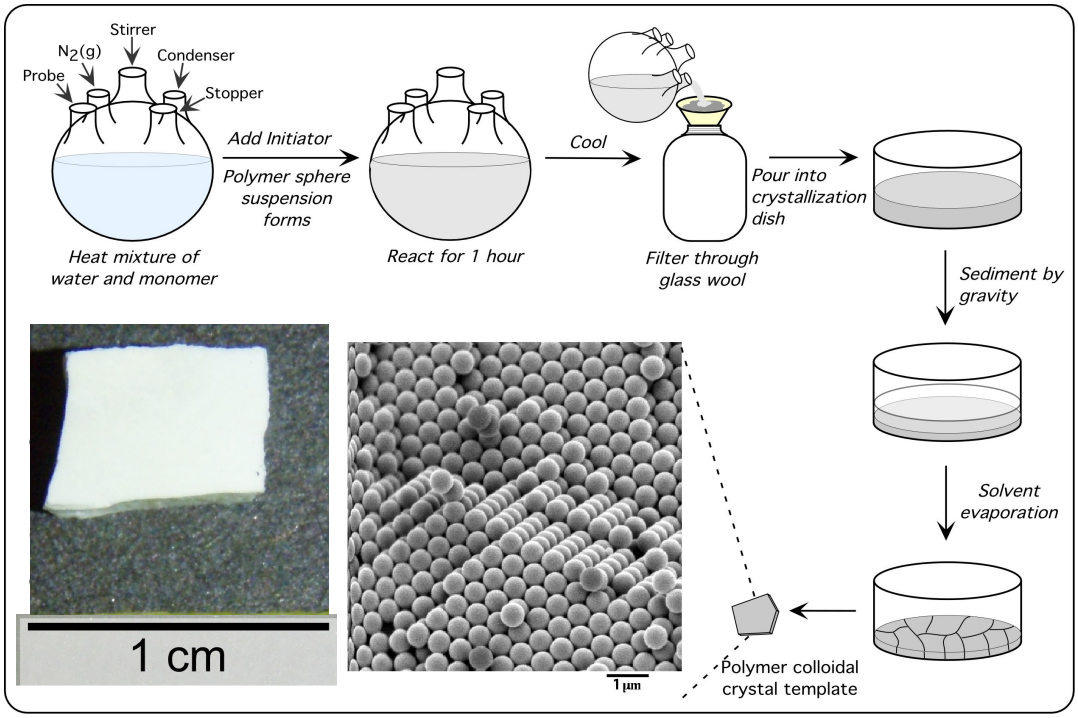

Figure A.1. Pictorial of PMMA sphere synthesis with a photograph of a KPS-PMMA colloidal crystal produced by sedimentation and a SEM image of the AMPA-PMMA sample. Image modified from reference [52].

A.1.1. AMPA and KPS synthesis

A.1.1.1. Materials

The following chemicals were used as-received: 2,2'-azobis(2-methylpropionamidine) (99+%), methyl methacrylate (99.9%) from Aldrich Chemical Company; potassium persulfate (certified) from Fisher Scientific; Millipore water with a resistivity 18.2 MΩ-cm was used. N_2 was obtained from the University of Minnesota house system.

A.1.1.2. Synthesis and products

Methyl methacrylate and H_2O were heated to 70 ºC or 75 ºC under a bubbling N_2 atmosphere, with a 300 RPM stir rate, until a stable temperature was reached in the PMMA reaction vessel[52]. 1 g of initiator was then added and the appearance of the solution changed from clear and colorless to cloudy and white. The reaction was allowed to continue for 2 h, now without N_2 bubbling. After 2 h the heating mantle was turned off and the solution was allowed to cool until 50 ºC, after cooling it was filtered through glass wool and stored as a colloidal suspension until needed for colloidal crystal formation.

Table A.1. Summary of variables in AMPA[52] and KPS[6] sphere synthesis.

Initiator	Temperature	Monomer amount	H_2O amount	Sphere size
AMPA	75 ºC	300 mL	1700 mL	428±10 nm
KPS	70 ºC	500 mL	1500 mL	540±9 nm

A.2. Colloidal crystal formation

While only one type of colloidal crystal was used, a number of types were synthesized. The sedimented samples were used throughout this work. Thin films fabricated by convective self assembly and rods prepared in capillaries were not useful to this study but may be useful in other applications.

A.2.1. Sedimentation

A colloidal suspension was poured into a crystallization dish and allowed to sediment over time (covered). This process took about 1.5 months for the spheres produced in this work. After the edges of the crystal appeared opalescent all the way to the top layer of sedimented colloids (through the crystallization dish), the cover was removed to evaporate the solvent. The colloidal crystal height produced was about 1/3 of the original suspension height. A typical colloidal crystal produced from this method can be seen in Figure A.1.

A.2.2. Convective self assembly

This technique was not used for the KPS or AMPA PMMA spheres. However both ~800 nm[122] and ~4 μm[123] sized spheres where obtained. These spheres settle too quickly for sedimentation techniques so convective self assembly was used instead.

Substrates, after cleaning in a basic piranha solution, were placed at an angle in a 5 dram vial. These vials were then filled up with a 0.5 wt% suspension of ~800 nm spheres or with a 2.0 wt% suspension of ~4 μm spheres. The vials were then placed in a sand bath with a temperature gradient of 60 ºC at the bottom of the vial and 50 ºC at the top. For the suspension containing 4 μm spheres, dry N_2 gas was passed over the vial at a rate of 2.5 $L \cdot min^{-1}$, aimed perpendicular to the front of the substrate to quicken the evaporation. This technique produced relatively ordered films over the course of 4 days.

This was adapted from techniques taught by Prashant Nagpal.

A.2.3. Capillary rods

Capillaries can help form filament-shaped monoliths. Holes were drilled into a vial cap and had approximately the same diameter as the capillary tubes (1.1 mm inner diameter). The number of capillaries that could be filled at one time was limited by the number of holes that fit in the cap. KPS or AMPA colloidal suspensions were poured into the vial, and capillary tubes (after cleaning in Nochromix) were placed in the holes in the cap. The vial was then placed on a 40 ºC surface for approximately one week before the solution was dry in the vial. The colloidal crystal rods could then be removed from the capillary with a thin wire. Typical colloidal crystal rods produced from this synthesis can be seen in Figure A.2.

This synthesis was adapted from Kamp et al.[124]

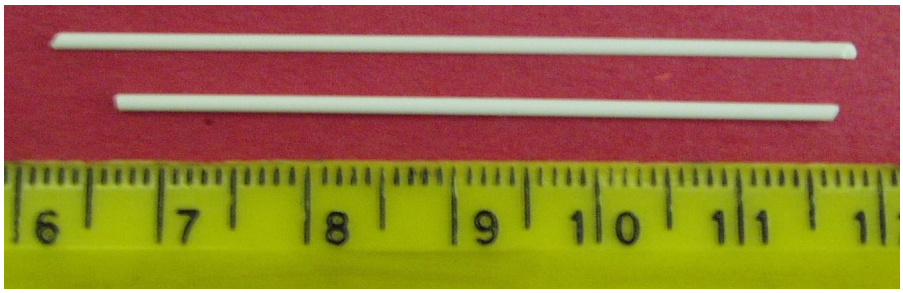

Figure A.2. Photograph of PMMA colloidal crystal rods from a capillary confinement technique.

Appendix B

Infiltration Techniques

Outline

B.1. Buchner funnel infiltration

B.2 Vacuum immersion infiltration

B.3. Drip coating

B.4. Multiple infiltrations

B.1. Buchner funnel infiltration

This infiltration technique was used for infiltrating WCl_6 into the colloidal crystal. PMMA colloidal crystal template was added to a solution of WCl_6 in a beaker with a ratio of generally 1 g to 2 mL respectively. The composite material was granular in nature when transferred to a Buchner funnel to remove the excess liquid. After the composite was dry, it was reduced to 3DOM W.

B.2. Vacuum immersion infiltration

To produce monolithic forms of 3DOM material the template must remain in a monolithic form after infiltration. All syntheses employing precursor solutions used this infiltration technique. To facilitate the retention of the monolithic form, the PMMA colloidal crystal was placed on the bottom of a filtration flask and evacuated for at least 1 h. After evacuation, precursor solution was added through a septum down the side walls of the flask. Dripping solution on the top of the colloidal crystal could cause the monolithic template to crack. The solution should never be added to a level higher than half the height of the colloidal crystal template. If a template was floating in the precursor solution, the amount of cracking in the monolith (up to the monolith falling apart) was increased immensely. After the monolithic composites were uniformly translucent, they were removed from the flask by lifting the composites out with a spatula. Using tweezers will crush the monoliths. The monoliths were then dabbed dried with a Kimwipe® to remove excess liquid from the surface and allowed to dry overnight before reduction for 3DOM W materials.

Adapted from Lee et al.[22]

B.3. Drip coating

For thin films and capillary rods, a drip coating method was employed as the structures are too thin for immersion infiltration by the method described in B.2. These templates required the addition of small droplets over the surface of the material. Once the material was uniformly coated, it was allowed to dry and then reduced, for 3DOM W materials.

B.4. Multiple infiltrations

Drip coating already employs multiple infiltration steps but it was uncertain if we could infiltrate more material into a template that had undergone vacuum immersion infiltration. For this technique two sets of templates were immersed in precursor solution at the same time. After immersion both samples were dabbed and allowed to dry. One sample was then drip coated two times (drying between coatings) to incorporate more precursor into the interstercial areas while the other sample was a control. The sample with 3 total coatings had an average pore size of 340±12 nm and the sample prepared by immersion only had average pore diameters of 300±15 nm.

From this we can conclude that multiple infiltrations increase the amount of precursor in the template and reduce the amount of overall shrinkage from the template dimensions to 3DOM material dimensions.

Appendix C

Characterization Techniques

Outline

C.1. SEM

C.2. XRD

C.3. ICP-mass spectroscopy

C.4. UV-vis reflectance

C.1. SEM

Scanning electron microscopy (SEM) was performed on a JEOL 6500 or JEOL 6700 Field-emission gun SEM with an accelerating voltage of 5–15 kV. Dimension on the SEM images were measured using ImageJ software (http://rsb.info.nih.gov/ij/). Only PMMA colloidal crystals were coated with 50 Å of Pt before imaging.

C.2. XRD

Powder X-ray diffraction (XRD) patterns were obtained using a Bruker AXS microdiffractometer with a 2.2 kW sealed Cu source, Hi-Star 2-D area detector and a 0.8 mm monochrometer. During the acquisition of the powder pattern, the XRD was set to 45 V and 40 A with a dwell time of 5 min per frame for data acquisition. Jade 6.0 and Jade 7.0 and Jade 8.0 software was used to process the XRD patterns. For crystallite size analysis, a LaB_6 standard was used to correct for peak broadening.

C.3. ICP-mass spectroscopy

Metal analyses were obtained on a Thermo Elemental PQ ExCell Quadrupole ICP-MS with simultaneous detector, Meinhardt nebulizer, Peltier cooled spray chamber and nickel cones. Analysis was performed by Mr. Rick Knurr.

C.4. UV-vis reflectance

UV-vis reflectance spectra were acquired using a Spectral Instruments 400 Series CCD Array UV-vis Spectrophotometer with a W filament source and a fiber optic probe at a 90° angle of incidence.